THE UNIVERSITY OF
NEW SOUTH WALES

**SCHOOL OF ELECTRICAL ENGINEERING
AND TELECOMMUNICATIONS**

Signals Processing of Electronic Warfare Systems

by

William Baxter

Thesis submitted as a requirement for the degree

Bachelor of Engineering (Electrical Engineering)

Submitted: October 27, 2016

Supervisor: Elias Aboutanios

Co-supervisor: Hamed Nosrati

Student ID: z3463372

Course Code: ELEC4121

Topic Title: Signals Processing of Electronic Warfare Systems

Student Name: William Baxter **Student ID:** z3463372

A. **Problem statement**

In a period where ESM systems are considered imperative tools in the use of military applications, the strategies behind modern warfare depend upon the techniques of telecommunications and EM surveillance. Knowledge of the origin of a signal of interest can dramatically affect the outcome of a military operation and can allow for offencive or defencive strategies to be devised accordingly. With the widespread implementation of many forms of ESM and surveillance systems, the environments in which these passive and active devices operate have become saturated with EM energy. As such, the direction and accuracy with which a signal of interest can be estimated becomes less than optimal. In light of this, it is necessary to devise a method with which to allow modern ESM systems to reliably estimate the DoA of a desired signal while ensuring its separation from an environment rich in EM interference.

B. **Objective**

Develop a Cramér-Rao bound (CRB) for a uniform linear array as a metric for performance estimation.
Incorporate the Spatial Correlation Coefficient (SCC) as a constraint so as to suppress interference effects.
Apply a maximum value to the SCC in combination with a manual windowing function to further regulate sidelobe levels.

C. **My solution**

Derivation of expressions pertaining to the CRB and SCC and solving using the optimisation method of Lagrange multipliers.
Solving non-linear equation set using MATLAB simulation software.
Comparing results from optimised configuration with initial configuration to determine overall improvements in performance.

D. **Contributions** (at most one per line, most important first)

Determination of expressions describing the CRB and SCC.
Development of code dedicated to mapping radiation response of a phased array system.
Interpretation of results and assessment of performance of optimised solution.
Worked collaboratively in the formulation of simulation code for the optimisation process.

E. **Suggestions for future work**

Refining of windowing function to improve regulation of sidelobe levels for oblique impingements.
Investigation of reflective interference effects from retrofittable architecture.
Improving efficiency of algorithm to optimise arrays with larger numbers of elements.

While I may have benefited from discussion with other people, I certify that this report is entirely my own work, except where appropriately documented acknowledgements are included.

Signature: William Baxter Date: 27/ 10 / 2016

Pointers

List relevant page numbers in the column on the left. Be precise and selective: Don't list all pages of your report!

10	Problem Statement
17-18	Objective

Theory (up to 5 most relevant ideas)

5	Antennas in Communications and Surveillance Systems
5-6	Electronic Warfare
6	Electronic Support Measures
7-10	Theory of Phased Arrays
10-11	Design Challenges

Method of solution (up to 5 most relevant points)

30-37	Derivation of expressions pertaining to the CRB and SCC and solving using the optimisation method of Lagrange multipliers.
37-38	Solving non-linear equation set using MATLAB simulation software.
49-56	Comparing results from optimised configuration with initial configuration to determine overall improvements in performance.

Contributions (most important first)

21-25, 30-37	Determination of expressions describing the CRB and SCC.
37-38, 67-70	Worked collaboratively in the formulation of simulation code for the optimisation process.
51-52, 55-56	Interpretation of results and assessment of performance of optimised solution.
70	Development of code dedicated to mapping radiation response of a phased array system.

My work

30-37	System block diagrams/algorithms/equations solved
N/A	Description of assessment criteria used
N/A	Description of procedure (e.g. for experiments)

Results

39-48	Succinct presentation of results
49-57	Analysis
51-52, 55-56	Significance of results

Conclusion

59	Statement of whether the outcomes met the objectives
57-58	Suggestions for future research

Literature: (up to 5 most important references)

30,21	[11] X. Wang, E. Aboutanios, M. Trinkle, M. G. Amin (2014)
27	[13] B. Ji-Hoon, K. Kyung-Tae, P.Cheol-Sig (2005)
29,34	[17] N.H. Noordin, T. Arslan, B. Flynn (2013)
28	[19] A. Moffet (1968)

Acknowledgements

I would like to acknowledge my supervisor, Elias Aboutanios, for the provision of his guidance and support throughout the duration of this thesis. I thank you for your endurance through the countless meetings I scheduled and e-mails I sent, and for helping me develop the knowledge to understand the niche topic that is radar.

My co-supervisor, Hamed Nosrati, was an absolute pleasure to work with. I am extremely grateful for the help you provided me during Elias' absence, as I would have been lost without your support. I appreciate the continual sacrifices you made to meet and discuss this thesis in person, and I hope that we work together again in the future.

Finally, I would like to acknowledge my family and friends for the reassurance and inspiration they have provided me over the academic years of my life. Many hardships were experienced and I thank them for helping me to persevere through the crucible that was this degree.

Abstract

The effects of interference on the estimation capabilities of electronic support measures can lead to ambiguities when performing direction finding and surveillance, increasing inefficiencies in the phased array. As military applications evolve, it is necessary to devise methods of reducing these ambiguities by improving the estimation capabilities of these arrays and their rejection of electromagnetic interference in the environment. For a low-cost electronic support measure, such as that desired by the author's employer, Jenkins Engineering Defence Systems, this will be achieved through a manipulation of the array geometry and signals processing techniques. Focusing on a linear array, the initial position of its elements will be optimised through a minimisation of the Cramér-Rao bound so as to improve its estimation capabilities for a particular direction of arrival. Given the potential for sources of interference in the system's operational environment, the Spatial Correlation Coefficient will be used as a design constraint to ensure a minimum rejection performance for a specific interference direction. By assigning a masking value to this Spatial Correlation Coefficient, we also achieve the regulation of sidelobe levels in the radiation pattern of the array.

Contents

List of Figures

1 Introduction

1.1 Antennas in Communications and Surveillance Systems

During the early 20th century, the discovery of electromagnetic (EM) waves led to the construction of the very first wireless communications systems. Beginning with the rudimentary Morse-code, advancements in the fields of electronics, signals processing and antenna theory catalysed the development of the radio and microwave systems that have become the familiar methods of modern communication. With over a century of improvement in these fields, significant demands have been made for further innovation in these media; specifically that of antenna design. Acting as the fundamental component in these communications systems, antennas have taken a variety of shapes and sizes in order to fulfil their contextual requirements. Despite these evolutions in their design, the very nature of an antenna's purpose has remained in its ability to provide for surveillance within the realms of three-dimensional space.

In the 1940s, reflector antennas consisting of a parabolic reflective plate connected to a feed antenna were initially used in commercial and military applications. Traditional accommodation for three-dimensional surveillance involved mechanically rotating the antenna on a pedestal in order to perform a scan of the surrounding environment. This proved suitable for conducting searches of the horizon and tracking airborne or grounded targets. The complexity of this scanning technique however, coupled with the reflector antenna's issues with gain, half-power beamwidth and radiation pattern, saw the need for a more versatile and sophisticated design.

The advent of World War II saw the introduction of the phased array antenna system. By systematically positioning antennas in an array, this configuration saw notable improvements in gain, half-power beamwidth and its radiation pattern; issues inherent with the previous generation of reflector antennas. By controlling relevant factors such as the configuration, element excitation, inter-element spacing and the number of elements used, the radiation pattern could be modified so as to conform to a specific purpose; as will be discussed further in Section 2. As a result, phased arrays have been used extensively in military applications over the years, such as illuminating targets with radiofrequency (RF) energy and assisting guided missiles. As electronics and signals processing techniques continue to improve, these systems have become a staple of modern surveillance and electronic warfare (EW) applications.

1.1.1 Electronic Warfare

The very concept of EW is defined as a "military action involving the use of electromagnetic energy to determine, exploit, reduce, or prevent radar use of the EM spectrum" [1]. In essence, the nature and operation of EW depends upon the capture of radar EM emissions using electronic intelligence (ELINT) devices, such as phased array systems. The radar received by these systems is able to be collected in support databases and

interpreted so as to extract useful information and to potentially program reactions against it. In this way, EW is divided into two categories: electronic support measures (ESM) and electronic countermeasures (ECM). With the efficiencies provided by modern surveillance applications, the primary focus of the EW community is then to passively gather intelligence in the form of EM energy of a system's surroundings and if need be, degrade radar capability. Given the nature of this study and its interest in passive surveillance, our attention will concern only that of ESM systems.

1.1.2 Electronic Support Measures

ESM systems fall under the section of EW concerning the actions undertaken in order to passively intercept, locate and analyse radiated EM emissions so as to exploit them in support of military operations. With its provision of EW information, ESM systems are seen as necessary precursors when conducting ECM, threat detection and obtaining situational awareness within an EM environment. It is typical of modern ESM systems to be comprised of multiple detection and measurement receivers and on-board processing capabilities to aid in the interception of radar emissions. Depending upon the technologies employed by the receivers, emitter locations and the direction of arrival (DoA) of stray radar signals can be determined via techniques such as difference time of arrival or phase difference rate. With improvements in signals processing theory, ESM systems also see the deinterleaving of signals so as to identify individual emitters in EM rich environments. This functionality makes ESM systems indispensable in the context of signals intelligence and when assisting in the decisions surrounding tactical responses and long-term operational planning.

The technology of the ESM being investigated in this paper is that of a phased array system. Section 1.3 details the conceptual and mathematical theory behind this form of array and their functions in the field of EW as an ESM.

1.2 Context

The work undertaken and presented in this study regards the potential for a passive low-cost phased array system to be developed and retrofitted to existing military structures. The motivation behind this choice of topic began as an initiative of the author's employer, Jenkins Engineering Defence Systems (JEDS). Functioning as a manufacturer of EW systems, JEDS has been involved with the maintenance and upgrading of many ESM systems aboard Australian and American military craft. These systems have become crucial in the aid of surveillance, allowing for the interception and analysis of EM energy for the purposes of threat detection around Australian borders and international regions.

Recently, JEDS became interested in the development of a compact array that could be readily attached to existing military structures. These structures vary from ship masts to aerial drones and personnel carriers, and intend to aid in the DoA estimation of transmitted signals at low economic cost. Smaller arrays such

as this are significant in reducing the profile of military electronic hardware with the additional benefit of allowing civilian law enforcement to achieve the accuracies in direction finding typically associated with their higher-grade military counterparts. A phased array system was selected by JEDS due to the advantages it holds over other conventional antenna systems and the ability for its characteristics to be altered via specific signals processing techniques. The versatility provided by the phased array makes them a suitable choice in the context of retrofitting, which is an area of expertise for JEDS.

1.3 Theory of Phased Arrays

An antenna is defined as "part of a transmitting or receiving system which is designed to radiate or to receive electromagnetic waves" [2]. In this regard, an array consists of a set of N spatially arranged elements whose configuration allows for superior reception of signals compared to a singular antenna. Due to this, phased arrays see much use throughout wireless and military applications.

Arrays can have as few as $N = 2$ elements, with the performance of the array typically improving as more elements are added. To this extent, it is common for higher-grade military surveillance systems utilising phased array technology to consist of hundreds of elements.

For analytical purposes, we assume that the origin of a transmitted signal, S, lies in the farfield relative to the phased array, i.e. $R > 2D^2/\lambda$, where R is the distance between S and the point of observance, D is the maximum linear dimension of the array with λ being the wavelength of the transmitted signal. This is visualised in Fiigure 1. These assumptions allow us to conclude that the EM waves falling onto the array possess a planar wavefront. As a result, the phase of the signal at each element will be a function of the arrival angle of the plane wave. By adding the signals together, the constructive and destructive nature of the addition allows the true bearing of the transmitted signal to be determined. The result of the addition of these signals at each element is called the "array factor".

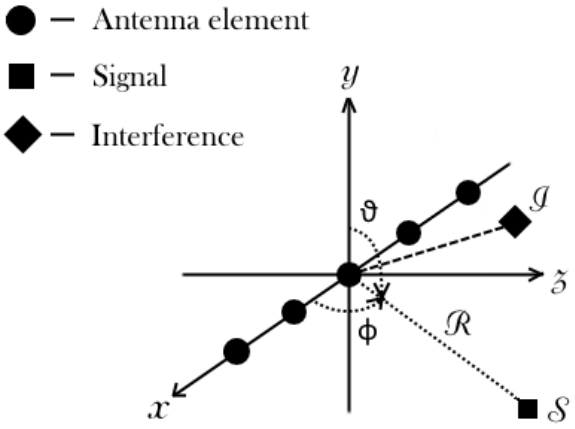

Figure 1: Structure of a uniform linear antenna array with its elements along the x-axis.

With a linear array, we may consider a Cartesian coordinate system with the three axes labelled as the conventional x, y and z, and the elements of the array placed along any of these major axes. In this regard, the spherical coordinate system is typically used in the analysis of antenna arrays. For this study, the array elements are positioned along the x-axis as shown in Figure 1 and conform to the farfield assumptions stated previously, with each element assumed to be isotropic; radiating uniform energy in all directions. With such an array consisting of N uniformly spaced elements separated by a distance d, the array factor can be described by the following equation:

$$AF(\phi, \theta) = \sum_{n=0}^{N-1} e^{-jk_0 nd \sin\phi \cos\theta} \tag{1}$$

where k_0 is the wave factor of the incident wave and ϕ and θ represent the azimuth and elevation angles respectively.

As we will be considering the signals propagating only in the xz plane, θ will yield the value of 0. Thus, the equation shown in (1) above can be expressed as:

$$AF(\phi) = \sum_{n=0}^{N-1} e^{-jk_0 nd \sin\phi} \tag{2}$$

The resulting radiation pattern described by (2) can be seen in Figure 2. Simulated in MATLAB using a uniform linear array with $N = 9$, the normalised amplitude in decibels has been graphed against the angle of arrival in degrees. It is immediately noticeable that at an angle of arrival of 0°, there is a maximum normalised response in the array factor. This peak in amplitude is called the "mainlobe" and is indicative of the angle of arrival of the transmitted signal relative to the array. The lower amplitude peaks surrounding the mainlobe are termed "sidelobes", and represent local maximums of unwanted radiation in various directions. As will be discussed later, these sidelobe levels must be restrained for surveillance and military applications in order to provide for improved angle of arrival estimations of transmitted signals.

A particular advantage of phased arrays is the ability for each signal at the elements to be summed and weighted accordingly, much like the Discrete Fourier Transform (DFT) algorithm present in conventional digital signal processing. By multiplying each signal by a complex phase and summing them together, the mainlobe of the radiation pattern can be steered; the array being electronically directed to point in another direction. This technique is called "beam steering" and improves the versatility of the array, allowing it to scan specific sectors of three dimensional space.

To this end, we may adjust the position of the mainlobe by multiplying (2) by the complex weighting factor:

$$w_n = e^{jk_0 nd \sin\phi_d}$$

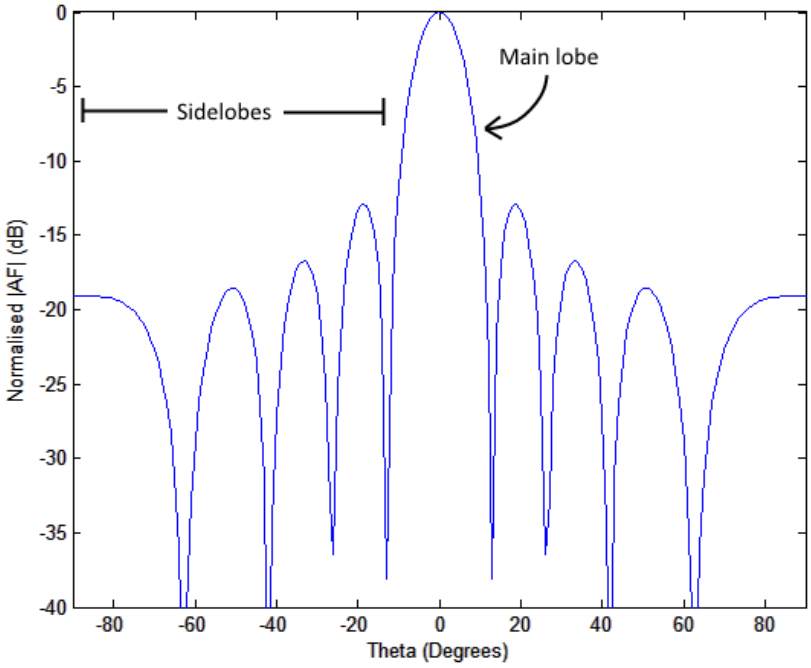

Figure 2: MATLAB simulation of the radiation pattern of an $N = 9$ element array.

where ϕ_d is the desired steering angle in degrees. Following from this, the array factor can be revised to accommodate for steering. From (2), we have:

$$\begin{aligned} AF(\phi) &= \sum_{n=0}^{N-1} w_n e^{-jk_0 nd \sin\phi} \\ &= \sum_{n=0}^{N-1} e^{jk_0 nd \sin\phi_d} e^{-jk_0 nd \sin\phi} \\ &= \sum_{n=0}^{N-1} e^{jk_0 nd(\sin\phi_d - \sin\phi)} \end{aligned} \tag{3}$$

Using the summation formula for a geometric series, we may finally express the array factor as:

$$AF(\phi) = \frac{1}{N} \frac{\sin\left(N\dfrac{k_0 d(\sin\phi_d - \sin\phi)}{2}\right)}{\sin\left(\dfrac{k_0 d(\sin\phi_d - \sin\phi}{2}\right)} \tag{4}$$

The expression in (4) above gives the form of the array factor that will be used for the mathematical modelling throughout the remainder of this study. Figure 3 below depicts the effects the value of $\phi_d = 30°$ has on the radiation pattern of the same $N = 9$ uniform linear array used above, with the mainlobe being shifted accordingly. It is evident that the phased array is now able to be electronically steered.

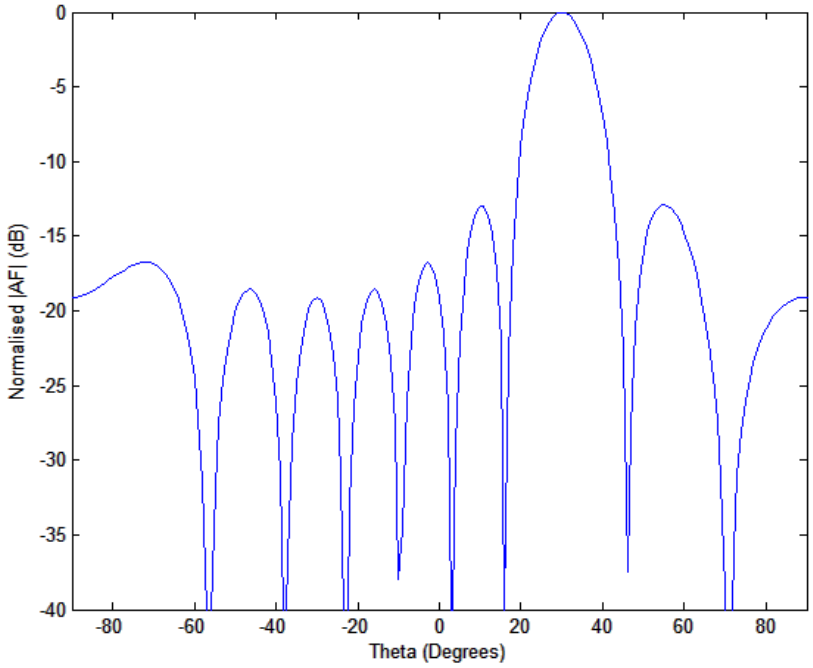

Figure 3: Radiation pattern of the same $N = 9$ linear array being steered to 30°.

1.4 Problem Statement

In a period where ESM systems are considered imperative tools in the use of military applications, the strategies behind modern warfare depend upon the techniques of telecommunications and EM surveillance. Knowledge of the origin of a signal of interest can dramatically affect the outcome of military operations and can allow for offencive or defencive strategies to be devised accordingly. With the widespread implementation of many forms of ESM and surveillance systems, the environments in which these passive and active devices operate have become saturated with EM energy. As such, the direction and accuracy with which a signal of interest can be estimated becomes less than optimal. In light of this, it is necessary to devise a method with which to allow modern ESM systems to reliably estimate the DoA of a desired signal while ensuring its separation from an environment rich in EM interference.

1.5 Design Challenges

Due to the nature of the phased array system desired by JEDS, suitable constraints are imposed on the design. As a result, a number of challenges present themselves in the development of a possible solution. These challenges are discussed in the following subsections.

1.5.1 Number of Antenna Elements

It is typical for phased array systems to be constructed using a large number of elements, with the accuracy with which the DoA of a desired signal can be estimated improving as more elements are used. However, as this phased array is to be implemented as a low-cost system, this sets a constraint on the number of elements that can constitute its aperture. As a result, the radiation pattern may potentially yield less accurate estimations as the width of the mainlobe will increase. To remedy this, the geometry of the array and the signals processing techniques used to perform the estimation must be optimised so as to alleviate this reduction in estimation performance.

1.5.2 Interference Effects

In order to derive accurate estimations of a transmitted signal's location, interference at the antenna aperture must be minimised. As mentioned in Section 1.4, the environment in which this array will be operating faces the possibility of becoming saturated from the multitude of EM signals propagating from active radar devices. In this regard, it is uncertain that the signal being detected by this passive system from a particular direction is truly the desired signal we wish to receive. To solve this ambiguity, we devise a method with which to separate multiple signals impinging on the array, allowing the system to reject the EM energy originating from a given direction. This will minimise interference effects and permit us to receive purely the desired signal.

1.5.3 Sidelobe levels

In Figures 2 and 3, the issues that sidelobe levels present in direction finding applications can be extrapolated. As sidelobe levels increase in magnitude, the mainlobe becomes less distinguished, compounding on the ambiguities introduced through interference effects. Such issues would hinder military applications, where accuracy is an absolute necessity. In addition, element spacings greater than a half-wavelength raise these sidelobes to magnitudes equal to that of the mainlobe; these special cases of sidelobes called "grating lobes". The nature of the array factor as defined by these sidelobes and grating lobes are directly influenced by the number of elements in the array, their configuration and the electronics or signals processing techniques associated with its design. It will be shown in Sections 2 and 5 that the uniform distribution of elements within a linearly phased array produces the highest sidelobes in its response, further highlighting the significance of optimising the array geometry. Due to their debilitating effects on direction finding applications, these issues have been subject to decades of research, with various methods of array optimisation being implemented. Such implementations will be further explored in Section 2.

1.6 Thesis Outline

This section has outlined the motivations behind this study and the theory that will be employed in the derivation of a proposed solution. The remainder of this thesis details the tasks undertaken throughout this study and is organised as follows. Section 2 details the research performed on past literature and identifies the various optimisation methods that have been adopted. Section 3 describes the objectives of this study, which sets the foundations for the proposed solution described in Section 4 and the methodology outlined in Section 5. These objectives stem from an analysis of the methods illustrated in the literature review. Section 6 presents the simulation results obtained from the implementation of the proposed solution, followed by Section 7, which functions as a discussion of these results. This study then concludes with Section 8 and a list of references and relevant appendices.

2 Literature Review

2.1 Non-uniform Arrays

The first forms of research regarding the performance of phased arrays date back to the 1960s. Due to the computing limitations present during the time, many of the early engineers and physicists adopted an analytical perspective. As such, most of their research focused on arrays with aperiodically distributed elements and their effects on performance. In 1960, Unz [3] studied arbitrarily spaced linear arrays, noting that improvements in performance were made using constant weights while manipulating the positions of the elements. Unz's approach could be extended to two and three-dimensional arrays, with his work forming the foundation for optimal array performance through non-uniformly spaced elements. King [4] then immediately performed further work on non-uniform array configurations, concluding that grating lobes could be replaced by sidelobes of lower amplitude than the mainlobe by using a controlled cosine method of element placement. However, King's many different methods of analysis provided only a quantitative study of the performance of non-uniform arrays. In 1961, Harrington [5] investigated the effects of small variations in the elements' positions in order to produce a desired geometry for the array. While he was able to reduce sidelobe levels by $\frac{2}{N}$ times the amplitude of the mainlobe, Harrington identified the unlikelihood of a simple optimisation procedure being formed for non-uniform arrays. While such early research focused on how the positioning of elements would yield an optimal radiation pattern, more recent research involved manipulating the directivity of these non-uniform elements in order to reduce sidelobe levels. Matzner et al. explored these effects [6], reducing sidelobe levels by inserting elements with higher directivity in the periphery of the array and elements with lower directivity in the centre. Although their simulation software was able to physically model the antennas and yield promising results, there was no mention of a specific method that would determine how many elements needed to be inserted and whether this could be extended to multi-dimensional arrays. Early research in the area of non-uniform arrays showed the benefits of introducing aperiodicity in array configurations, however none of these methods utilised an optimisation algorithm to determine the optimal degree of offset for each element. This concept of non-uniformity would become the subject of many decades of research.

2.2 Biological Algorithms

As computing power improved, the optimisation of array geometry could be derived using biological algorithms. Such complex algorithms aimed to determine an optimised geometry through performing Monte Carlo simulations, discarding less effective solutions through virtual evolutions. In 1997, Yan and Lu [7] utilised a modified Genetic Algorithm (GA) that represented array weighting vectors as complex number chromosomes. This implementation reduced processing time and could be applied to arbitrary arrays, allowing for constraints to be imposed on their design. Khodier and Christodoulou [8] took an alternative approach to Yan and Lu,

utilising Particle Swarm Optimisation (PSO) with constant weights to discern optimal element positions. While conventional biological algorithms manipulated the array as a whole, Wang et al. [9] approached the issue of sidelobe reduction by optimising subarrays within a planar structure and staggering their rows. Despite lowering sidelobe levels considerably, this came at the expense of high computational complexity. While biological algorithms prove an effective means of minimising sidelobe levels, their applications to this problem and the results obtained can be compared to the optimised cost functions later discussed.

2.3 Adaptive Arrays

With improvements in the fields of electronics, the concept of adaptive arrays were developed. In such arrays, all elements are used in the provision of a coarse (approximate) direction of arrival estimation of transmitted signals. Following this, elements in the array have their weightings adjusted so as to reform the beam pattern and refine the angle of arrival approximation. This technique, often termed "adaptive beamforming", was investigated by Wu et al. [10], who compared the two conventional sidelobe level control methods used by adaptive arrays: Integrated Peak Sidelobe Control (IPSC) and Distributed Peak Sidelobe Control (DPSC). Despite showing that the former method outperformed the latter, both methods were compared using only uniform arrays. In the context of non-uniform arrays, it was noted that the optimisation algorithm would prove difficult to solve. Aboutanios et al. [11] approached adaptive arrays from an optimisation perspective, developing a Spatial Correlation Coefficient (SCC) which when minimised, would yield an adaptive array with a high signal-to-noise ratio using fewer elements. Furthering this optimisation, subarrays were selected within the main array so as to reduce interference effects. Adaptive array technology could prove useful in this study due to its ability to filter out interference and jamming effects, however, the full potential of adaptive arrays are typically realised when using a larger number of elements than those constrained by this low-cost system.

2.4 Optimisation Algorithms

In conjunction with the methods employed by biological algorithms, the interest garnered by the potential for non-uniform arrays led to various studies utilising cost functions to more rigorously determine optimal non-uniform geometry. While earlier research experimented with offsetting elements from their initial positions, recent studies implemented various optimisation algorithms in order to accurately determine how element spacing should be varied. Jiao et al. [12] utilised the constrained non-linear optimisation method to meet a specified sidelobe level while achieving maximum directivity. In the scenario that this criteria could not be met, their technique produced a set of array coefficients yielding the best attainable sidelobe level and directivity. It was noted however that the issue of cross-polarisation was not addressed in their implementation, with their results yielding a high amount of pattern distortion. Similarly, Bae et al. provided a form of pattern

synthesis for linear arrays using the Gauss-Newton method [13], however without the pattern distortion that was present in Jiao et al.'s results. By optimally adjusting the elements from their initial positions obtained via Fourier transforms, the inner and outer sidelobe levels were reduced in the resultant radiation pattern. These reductions in sidelobe levels however were only possible with a scanning range of $-30^\circ \leqslant \theta \leqslant 30^\circ$ along the azimuth. Alternative to these methods, Gazzah and Abed-Meraim derived a Cramér-Rao Bound (CRB) for the direction of arrival estimation in order to determine an optimal array geometry [14]. In solving the optimisation algorithm, ambiguities in direction finding were reduced, however the configuration of the array was limited to the shape of a curve. With the success of using a cost function to optimise array geometry, the application of such a method sees use in the development of a solution in this study. This is magnified by the fact that a minimal number of elements will be used and so the inter-element spacing for a non-uniform configuration must be devised accurately.

2.5 Phase Tapering and Windowing Functions

Advancements in signals processing theory saw the application of phase tapering and windowing functions to the array factor in order to reduce sidelobe levels in the array's outer elements. Early implementations of phase tapering saw the manual reversal of the phase towards the ends of the array [15, 16]. Smith et al. achieved such a novel technique in 1983 by applying a 0 or π phase shift at each array element [16], successfully minimising sidelobe levels. However, it was assumed that a look-up table would be used to discern which elements exhibited reversed phases; the size of this look-up table growing with the number of elements in the array. The effects of windowing on the sidelobe levels have also been investigated [17, 18], with Noordin et al. applying a variety of windowing techniques to 3-faceted arrays. This method was also implemented by Sarker et al., albeit to linear, circular and planar arrays. Both forms of research concluded that the Blackman window was the most effective in suppressing sidelobe levels in the outer elements of the array. It was noted that depending on the windowing function, a compromise must be made between the mainlobe beamwidth and the sidelobe levels. Noordin et al. further stated that the Kaiser window with a weighting of $\alpha = 3$ produces the best balance between sidelobe levels and mainlobe beamwidth. This form of sidelobe level reduction using windowing functions would prove a suitable implementation in the design of this low-cost system due to its ability to reduce sidelobe levels in arrays consisting of a minimal or maximal amount of elements.

2.6 Minimum-redundancy Arrays

With the development of non-uniform arrays and the cost functions yielding optimal inter-element spacings, the presence of redundant elements within a linear configuration were first explored by Moffet as early as 1968. Given an N element uniformly spaced array, Moffet realised that there were a high number of redundant spacings between elements. By reducing these spacings, a higher resolution could be achieved which

would permit the length of the array to be increased [19]. Through the formulation of an optimisation ratio, specific elements within conventional non-uniform arrays could be discarded. As a result, the non-uniform minimum-redundancy arrays possessed a higher resolution than their conventional non-uniform counterparts while utilising fewer elements. A notable disadvantage of minimum-redundancy arrays however was that the resolution of such arrays could not be increased by adding elements; a problem whose difficulty was mentioned by Moffet. The practical applications of minimum-redundancy arrays were investigated by Liqiang and Houde, who studied the direction finding ambiguities associated with them [20]. By formulating the redundancy ratio in a similar manner to Moffet, Liqiang and Houde devised minimum-redundancy arrays for various numbers of elements. Performing simulations using a 4-element minimum-redundant array, it was discovered that its direction finding performance exceeded that of its conventional non-uniform counterpart, with its radiation pattern correctly identifying the angle of arrival of closely spaced signals. The issues Moffet described were also present in Liqiang and Houde's paper, with their redundancy calculations reaching a maximum of 10 elements.

3 Thesis Objectives

The objective of this thesis is to determine the array structure that provides the optimal performance for a particular DoA, while ensuring a minimum rejection performance to an interfering direction and the regulation of sidelobe levels. To accomplish this, a suitable cost function is derived that permits us to achieve the required performance. As such, the problem was deconstructed into milestones, whose details are itemised below:

1. Develop a Cramér-Rao bound (CRB) for a uniform linear array as a metric for performance estimation.
2. Incorporate the Spatial Correlation Coefficient (SCC) as a constraint so as to suppress interference effects.
3. Apply a maximum value to the SCC in combination with a manual windowing function to further regulate sidelobe levels.

It is important to mention that the objectives as originally stated at the beginning of this study have been adjusted to those shown above. Throughout this thesis, many alternate methods of implementation were investigated for the solution portrayed in Section 4. As a result, the objectives of the thesis remained dynamic until a specific methodology was able to be developed and consolidated via the means of simulation, as detailed in Section 5. The overall aim of the thesis, however, has remained unchanged, with the goal of optimising the performance of a system involved in electronic warfare, specifically that of a linearly phased array.

When retrofitting the array to existing structures, a linear configuration for this system would yield the most flexible in conforming to various architectures. Given the few elements in the array due to its low-cost nature, the effects of element positioning on the radiation pattern must be used to its full potential. Previous literature has shown that phased arrays consisting of non-uniform spacings exhibited improved radiation patterns over their uniform counterparts. As a result, spacing the elements linearly in a non-uniform fashion would prove appropriate for this study. It is imperative then that a method of optimisation be determined using the CRB, as this would allow for a set of element positions to be formulated that would result in the most optimal performance in regards to DoA estimation. This optimisation in performance using the CRB was investigated previously by Aboutanios et al. and Gazzah et al., who both were able to reconfigure the aperture of an initially uniform array so as to aid DoA estimations. The derivation of the CRB and the reason for its use within the proposed solution will be discussed further in Section 4.2.

The proposed solution would ideally see much use within military applications, given its function of surveillance within EM environments. It is natural to assume then that the system would be subject to a multitude of signals if it were to operate within an environment rich in EM energy. As discussed in Section 1.5.2, to supplement the optimisation of the element positioning described in the first objective, the system must be able to separate multiple incoming signals from its surroundings, where there may be the possibility of

intentional or unintentional interference effects. To achieve this, the SCC is imposed as a constraint on the determination of the CRB so as to allow for signals to be made distinct from one another. The use of the SCC as a mechanism to separate multiple signals is a novel application studied by Aboutanios et al., with their results successfully isolating a desired signal from unwanted interference [11]. Section 5 details the implementation of the SCC as a form of rejection criteria for a particular angle of arrival of interference, and its ability to allow the optimised system to hone in on a specific DoA.

With the optimised system intending to achieve the element positioning that will determine a balance between estimation performance and signal separability, the reduction of sidelobe levels is a necessary objective in order to further distinguish the mainlobe of the radiation pattern. To achieve this, a masking value is to be assigned to the SCC, i.e. a maximum value of the SCC over a range of angles. This way, we are able to impose an additional restriction that the magnitude of the first sidelobe level is permitted to achieve. This is combined with a manual windowing function to further regulate these levels, as described in Section 5. This combination of masking the SCC and the use of a windowing function are necessary implementations due to the few number of elements being utilised in this solution, which would naturally yield higher magnitudes of sidelobes.

4 Proposed Solution and Considerations

As described in Section 3, the objectives of this work involve optimising the configuration and signals processing techniques of a linear array so as to improve its performance. With these objectives in mind, the proposed solution will position the elements of a linear array by utilising a cost function that combines the CRB and the SCC. As will be discussed in Section 5, by assigning the SCC a maximum value, we are able to satisfy a rejection criteria for a specific interference direction while regulating sidelobe levels. This improves the versatility of the array and provides a balance between these dual capabilities. The array factor of the optimised linear array will then be subject to a manual windowing function to further regulate the first sidelobe level in the radiation pattern.

It has been shown through an investigation of the literature that alternate methods of solving the problem at hand exist, however only few with the specific objective of this study. Many forms of the literature focused on singular aspects, such as the optimisation of array geometry or the specification for a particular rejection criteria; very few attempting to combine estimation performance with signal separability.

Due to the nature of this system, many of the choices regarding its theoretical and analytical design were influenced directly by its specific purpose as an ESM. This required making a distinction between the two primary functions of modern ESM systems, estimation and detection, and determining which of these our system would be accommodating for. This was an important distinction to make, as the optimisation methods were dependent on what functions the array was to provide. The following subsections elaborate on this distinction and the design choices stemming from it; these sections providing an analysis of their significance in regards to a viable solution.

4.1 Estimation vs. Detection

Modern ESM systems serve to either estimate the direction of arrival of incoming signals or to detect which of them lie above a certain threshold. Superficially, the assignment of the system to the appropriate function appears rather trivial, however, slight differences between these two forms manifest themselves in the process of optimisation.

When optimising a system designed for estimation, the width of the mainlobe is of primary concern. Considering that an array's direction finding capabilities are directly linked to its radiation pattern, it is clear that the span of the mainlobe and its ability to be distinguished from the peripheral sidelobes is significant. As such, to more accurately estimate the direction of arrival of a source, the array factor of the system should possess a more narrow mainlobe width, as visualised in Figure 4.

For a system designed for detection, the width of the mainlobe is not as critical as for a system performing estimation. When detecting a variety of sources, those signals whose amplitudes lie above a specific threshold

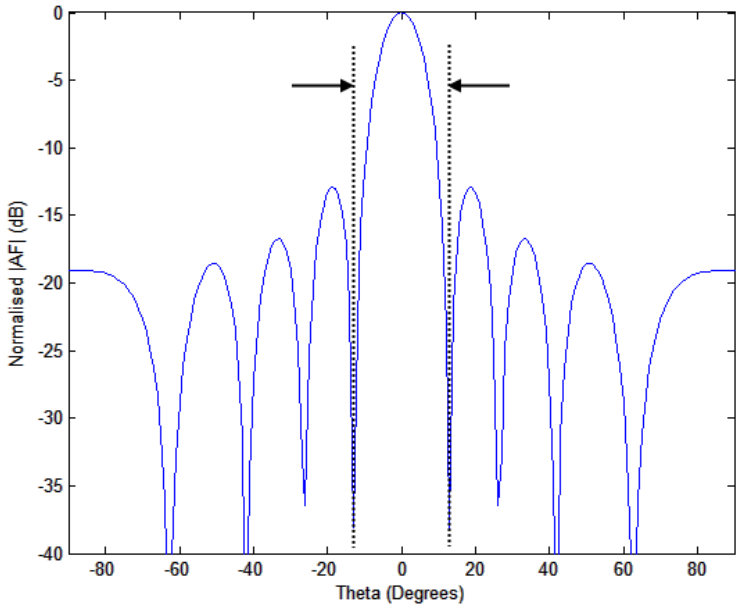

Figure 4: Depiction of the width of the mainlobe and its significance in a system designed for estimating direction of arrival.

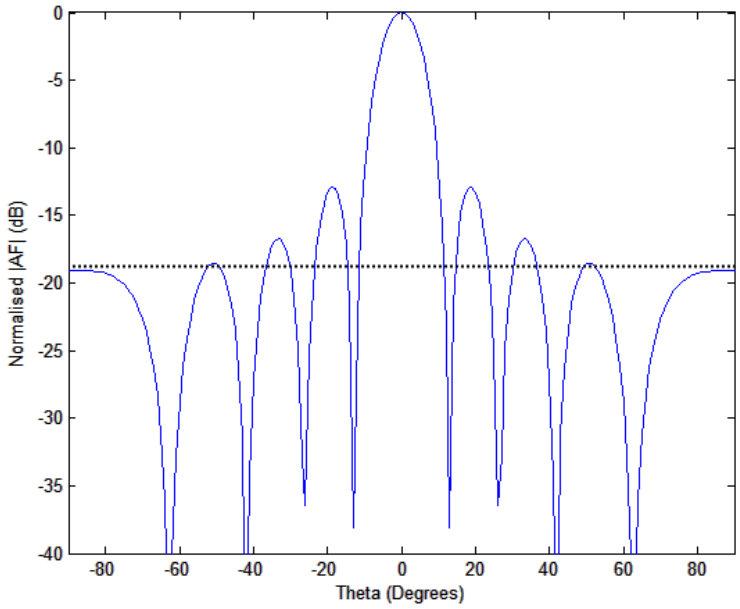

Figure 5: Depiction of the valid regions lying above a specified threshold level in the radiation pattern of a system designed for detection.

value will be deemed as valid readings, with those under the threshold value discarded. As shown in Figure 5, rather than the width of the mainlobe being of primary importance, the choice of threshold value and the peak-sensitivity of the array are the more applicable factors for those systems specialising in detection.

In the context of this problem, the phased array system desired by JEDS focuses on estimation rather

than detection. Considering their intention to use the system to accurately identify the direction of arrival of incoming signals, it is clear that a narrow mainlobe is required. As discussed in Sections 1.3 and 3, a higher number of elements in the configuration corresponds to a reduced mainlobe width in the array factor. Since this system is designed to be of low economic cost, the distinction between estimation and detection allowed for suitable methods of optimisation to be explored. Given the few number of elements we would be using compared to conventional phased array systems, optimisation using the CRB was selected as the most appropriate method for this problem. This is discussed further in the following subsection.

4.2 Fisher information matrix and the Cramér–Rao bound

In the fields of estimation theory and statistics, the ability to estimate a certain set of parameters without regard to those unknown sets responsible for influencing the collected data is described by the Fisher information matrix and its inverse relation, the CRB. When a deterministic model of a spatially incoherent system has been discovered, such a model should consist of the parameters that are affecting the measured signal. Consequently, the Fisher information is then a measure of the amount of coherent data received from a measured signal relative to a given parameter. Through its inverse relation, the CRB then constructs a lower bound on the variance of any unbiased estimators of this given parameter within the system.

Through the inverse relationship that exists between the Fisher information and the CRB, the estimation of these parameters is directly related to the system's sensitivity to these parameters and the sensitivity's orthogonality to those unknown sets influencing the data. As such, the CRB possesses the following characteristics:

- If an estimator achieves the lower bound imposed by the CRB, we are confident that the estimator is a Minimum-Variance Unbiased Estimator (MVUE); an unbiased estimator that has a lower variance than all other possible estimators for that parameter.
- The CRB is able to function as a benchmark upon which the performances of other unbiased estimators can be gauged.

In this way, the bound indicates that the variance of any unbiased estimator is at least as high as the inverse of the Fisher information.

The Fisher information and the CRB are highly applicable tools in the construction of the optimisation methods associated with this problem. For this system, it is evident that the received signals may be supplemented by elements of noise, given the environment in which this low-cost ESM will be implemented. It was shown in the previous literature in Section 2 that the effect of array geometry on the radiation pattern is of great significance. With an unoptimised geometry, considerable noise independent of that combined with the signal is able to be introduced into the system's response. As such, by using the Fisher information in accordance with the CRB, we are able to derive how much information the position of the array's elements contains about

the DoA of the incoming signal; the more information it contains indicating a stronger dependence between these two parameters.

While other methods of optimisation have been used in the past to improve array performance, many of those arrays utilised up to 30 elements. As shown in Section 1.3, arrays consisting of a higher number of elements produce responses possessing a narrower mainlobe. The direction finding capabilities of such dense arrays would prove more effective than the minimal number of elements being utilised in this system. As such, it was imperative to discern how to more accurately determine the DoA of a source when the mainlobe would be comparatively wider due to these fewer number of elements. It follows naturally that by using the Fisher information and the CRB, a relationship between element positioning and the received signal is able to be determined. This serves of great use in our context, as given the few elements constituting this ESM, their positions would have to be carefully chosen so as to optimise the response of the array. As it is this response that determines the accuracy with which we can pinpoint a source's direction of arrival, the Fisher information allows us to establish a relationship between the accuracy of the received signal and the positions of the elements. As will be shown in Section 5, the CRB enables us to derive this relationship and to maximise the array's performance and efficiency.

4.3 Spatial Correlation Coefficient

As will be shown in Section 5, the optimised array structure determined by the CRB includes the boundary antennas, which guarantees the largest aperture. However, these boundary antennas typically cause arrays who have their geometric centres positioned about the origin to exhibit high sidelobes. In order to remedy this, we impose an additional constraint on the design problem in the form of the SCC.

In wireless communications and surveillance systems such as this, multiple antenna elements are used in both the transmitting and receiving systems so as to improve overall performance. This improvement is gained by precoding the multiple statistically independent channels that exist between each transmitting and receiving antenna pair with identical characteristics; increasing the system's reliability. The channels between these different antenna pairs are often spatially correlated, as a correlation typically exists between the desired signal's spatial direction and the average received signal gain.

In the context of this design problem, given that the array configuration is a fundamental factor affecting the performance of the system, we may use the SCC to express the spatial separation between the desired signal and external interference effects. In effect, by combining the constraint imposed by the SCC with the lower bound derived by the CRB, we are able to not only control the array's estimation capabilities, but also allow for multiple incoming signals to be separated from one another by determining the correlation between their spatial directions. The trade-off between the two forms of optimisation is visualised in Figure 6. With these constraints imposed on the initial array, we can balance the array's performance characteristics.

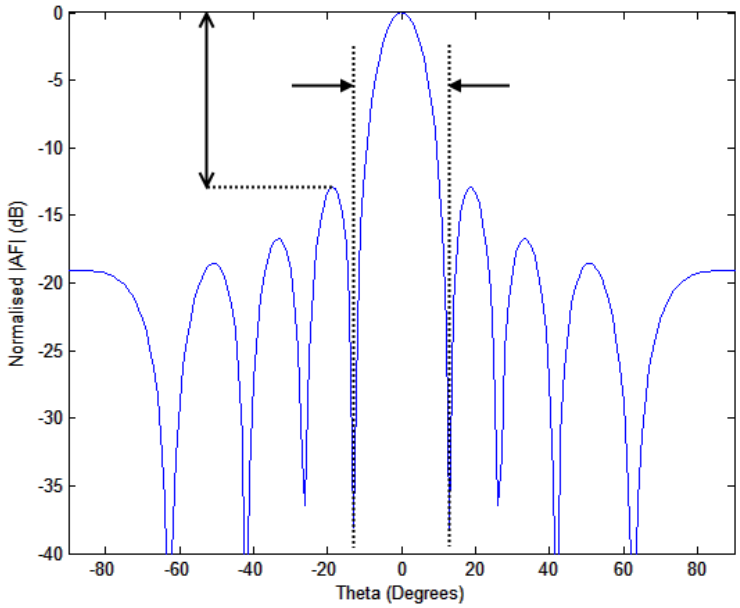

Figure 6: Depiction of the trade-off between the estimation performance (mainlobe beamwidth) and the sidelobe levels.

To further the constraints imposed by the SCC, by assigning it a maximum masking value, we inherently impose a maximum magnitude that the first sidelobe level is permitted to obtain within the response of the system. This effectively regulates the magnitude of the sidelobe levels across a range of angles, acting in conjunction with the separation of a desired signal from a direction of interference.

The formulation of the problem as a joint cost function involving the CRB and the SCC allows the system to endure any future changes to its design or function. In its current state, as a low-cost ESM system, we are able to improve direction finding capabilities while minimising interference effects. However, if the ESM were to ever disregard economic cost and opt to incorporate a larger number of elements, the masking value assigned to the SCC can be decreased, given that the increased element count would correspond to a natural reduction in sidelobe levels near the mainlobe and the boundaries of the aperture. This gives further credence to the inclusion of the SCC as it allows for systems possessing a varied number of elements to still maintain some form of regulation over their peak sidelobe levels once their positions have been optimised. By changing the value of the masking applied to the SCC component of the cost function, the array is effectively able to adapt to the number of elements it is composed of.

4.4 Optimisation using the method of Lagrange Multipliers

A problem such as this has its roots embedded within mathematical optimisation, which is the process of selecting the best element from a set of alternatives in accordance to some constraint or performance criteria. This is typically done by maximising or minimising a function through the choice of input values

pertaining to a set satisfying the constraints, and computing the value of the function. In this way, the process of mathematical optimisation is able to determine the "best" value of some function within a well-defined domain.

The method of Lagrange multipliers is a powerful form of optimisation that is able to achieve this goal of maximising or minimising a function subject to equality constraints. In general, the Lagrangian is defined as the sum of the objective function and the product of its relevant constraint function and a 'Lagrange multiplier', typically denoted by λ. To this end, we are able to consider that for the following generalised optimisation problem,

$$\begin{aligned} \min \quad & f(x,y) \\ \text{s.t.} \quad & g(x,y) = c \end{aligned} \tag{5}$$

its corresponding Lagrangian function can be expressed as:

$$\mathcal{L}(x,y,\lambda) = f(x,y) + \lambda g(x,y) \tag{6}$$

where $f(x,y)$ and $g(x,y)$ are the objective and constrained functions respectively in terms of the variables x and y, with the intention of minimising$f(x,y)$ subject to $g(x,y) = c$ for some constant c. The value of x and y that maximises $\mathcal{L}(x,y,\lambda)$ is dependent upon the multiplier λ.

The method of Lagrange multipliers makes use of the intuition that if we were to stand at the maximum of the objective function $f(x,y)$, it cannot be increasing at any nearby point where $g(x,y) = c$. If this wasn't the case, we would be able to continue along the path of $g(x,y) = c$ to climb higher along the curve, implying that our starting position was not actually the maximum value. The same concept applies in the minimum case, if we were to be standing at the minimum of the objective function. This highlights the significance of the starting position when attempting to use the method of Lagrange multipliers, and how results can vary depending upon the value of the constrained function and where the starting position is chosen to be. The method by which the Lagrange function is to be solved employs the following process:

1. Find the partial derivative of $\mathcal{L}(x,y)$ with respect to each of the variables constituting the function, i.e. x and y, and the Lagrange multiplier λ.
2. Set each of these partial derivatives equal to 0, such that $\frac{\delta}{\delta x}(\mathcal{L}(x,y,\lambda)) = 0$, $\frac{\delta}{\delta y}(\mathcal{L}(x,y,\lambda)) = 0$, $\frac{\delta}{\delta \lambda}(\mathcal{L}(x,y,\lambda)) = 0$. Substitute the solutions for x and y so as to express $\frac{\delta}{\delta \lambda}(\mathcal{L}(x,y,\lambda)) = 0$ in terms of λ only.
3. Solve for λ and use this value to determine the optimal values of x and y.

For this particular problem, the method of Lagrange multipliers proves a suitable application for the minimisation of the combined CRB and SCC functions. With the problem designed to minimise the CRB (or

conversely, to maximise the Fisher information) using the SCC as a form of criterion, the problem can be stated as a constrained minimisation and solved accordingly, as will be shown in Section 5.

4.5 Equation solving algorithms in MATLAB

In order to solve the set of non-linear equations obtained by taking the multiple partial differentiations of the Lagrangian, the 'fsolve' function inside of MATLAB is utilised. When MATLAB is provided with a set of non-linear functions $F_i(x)$, its solution to the set of equations is the determination of a vector x that renders all $F_i(x) = 0$. This concept is adopted by the fsolve function, which attempts to solve a given system of equations by minimising the sum of squares of its components. If the sum of squares is equal to 0, MATLAB effectively renders the system of equations as solved. To determine a solution to this given system of equations, MATLAB employs the use of a large-scale trust-region algorithm.

The trust-region approach is a form of optimisation that represents a particular region of an objective function that is approximated by a model function. In its simplest terms, the trust-region method is able to approximate an objective function f using a simpler function q, which acts as an acceptable reflection of the behaviour of f within the neighbourhood N surrounding the point of interest x. It is this neighbourhood that is defined to be the trust-region, with a step of size s computed by minimising over the neighbourhood N. The sub-problem posed by the trust-region is able to be expressed as:

$$\min_{s} \quad q(s), \quad s \in N \tag{7}$$

The current point is updated to $x + s$ if $f(x + s) < f(x)$. Otherwise, the current point remains unchanged and N is shrunk, with the step being repeated. This method of trust-region approach is an effective means of determining the solutions to the set of non-linear equations derived from (6).

It can be extrapolated that for more complex optimisation procedures, performing this analytically would prove an insurmountable task. The following section will detail the methodology employed in the implementation of the proposed solution.

5 Methodology

The method by which the proposed solution was implemented was chronological in nature. As detailed in Section 4, the process of determining which mathematical optimisations and mechanisms would allow for a successful implementation was deductive, with many of the algorithms being selected due to the way in which the problem was formulated and their suitability to the application.

Having identified these algorithms, the method was broken down into sections, with each reflecting a specific objective as detailed in Section 3. The methodology depicted in this chapter moves sequentially through these objectives, beginning with an investigation into array geometry and then moving towards the implementation of the relevant optimisation algorithms. In this way, a coherent method was formed and a viable solution was achieved.

5.1 Investigation of Array Geometry and Windowing Functions

5.1.1 Array Geometry Manipulation

The methods outlined in the most relevant literature became the subject of ongoing simulations, with array geometry manipulation and weighting methods being experimented with. In order to visualise the impact of these techniques on the radiation pattern, a model of the phased array had to first be constructed. Using Equation 3, the array factor defined in Section 1.3 was implemented using MATLAB, providing a base model from which all simulations could be conducted, whose results will be discussed below. In all simulations, the signal frequency was set to 1 GHz, with $k_0 = \frac{2\pi}{\lambda}$, where λ was the wavelength of the signal.

In order to verify the significance of an array's geometry upon its performance, the methods outlined in the previous literature were consulted. Previously, Bae et al. applied the Gauss-Newton algorithm so as to optimally adjust the initially uniform array elements obtained from a Fourier transform based formula. For an $N = 17$ element array, these adjustments produced the optimal non-uniform configuration, as outlined in their study. To verify the resultant reduction in sidelobe levels induced by non-uniformity in the array, the patterns produced by both the optimal 17-element non-uniform linear array and its uniform counterpart were compared, with the inter-element spacing being set to $d = \lambda/2$ in the uniform case. With both arrays steered to 0°, it can be seen in Figure 7 that the mainlobe of both arrays are identical, possessing the same beamwidth. It is also immediately apparent that the first two sidelobe levels of the non-uniform array are lower than those of their uniform counterpart, with both arrays possessing the same number of sidelobes. Although some sidelobe levels of the non-uniform array exceed those of the uniform, the overall effect of sidelobes has successfully been reduced by adopting a non-uniform configuration.

It is clear that the configuration of array geometry is fundamental to its performance, with a technique such as this proving significant in the development of the low-cost ESM system. The optimisation of the positioning

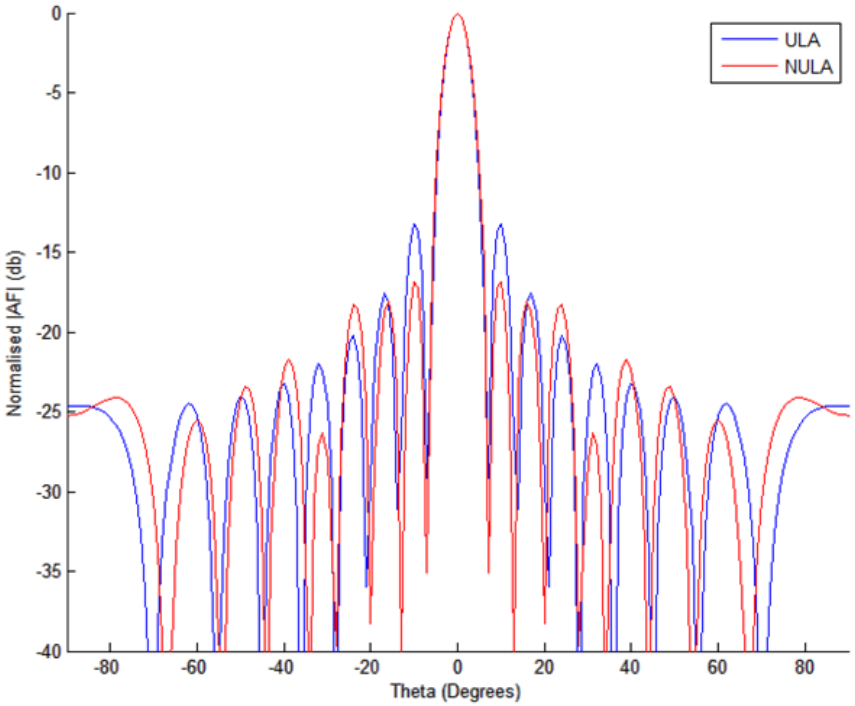

Figure 7: Radiation pattern of Bae et al.'s optimal $N = 17$ non-uniform linear array (red) and its $N = 17$ uniform counterpart (blue) with both steered to 0°.

of elements will be experimented with so as to improve estimation performance via a reduction in mainlobe beamwidth.

In addition to the work done by Bae et al. being used as a form of verification of the effects of array geometry, the concept of minimum-redundancy linear arrays were also investigated. It was initially thought that these forms of arrays would be largely relevant to this study due to the small number of elements utilised in their configuration. As the low-cost ESM system will also be using a minimal number of elements, it was necessary to simulate the performance of these minimum-redundancy arrays and gauge their application to this study. The model used in this simulation was derived by Liqiang et al., who compared the direction of arrival estimation of minimum-redundancy arrays to common non-uniform linear arrays. Figure 8 compares the radiation patterns obtained using a 4-element common non-uniform linear array and its corresponding minimum-redundancy array, as devised by the literature.

It is apparent in Figure 8 that the minimum-redundancy array produces fewer sidelobes compared to its counterpart, albeit possessing a much higher average magnitude. It is immediately noticeable however that the minimum-redundancy configuration has significantly reduced grating lobes; minimising the inefficiencies towards the ends of the aperture. In terms of estimation performance however, it is clear that the mainlobe of the minimum-redundancy array is wider than that of its corresponding non-uniform linear array. This poses an issue for our solution, as to achieve the best possible estimation performance, the width of the mainlobe must be reduced. While the grating lobes have been suitably suppressed, it is evident that the estimation

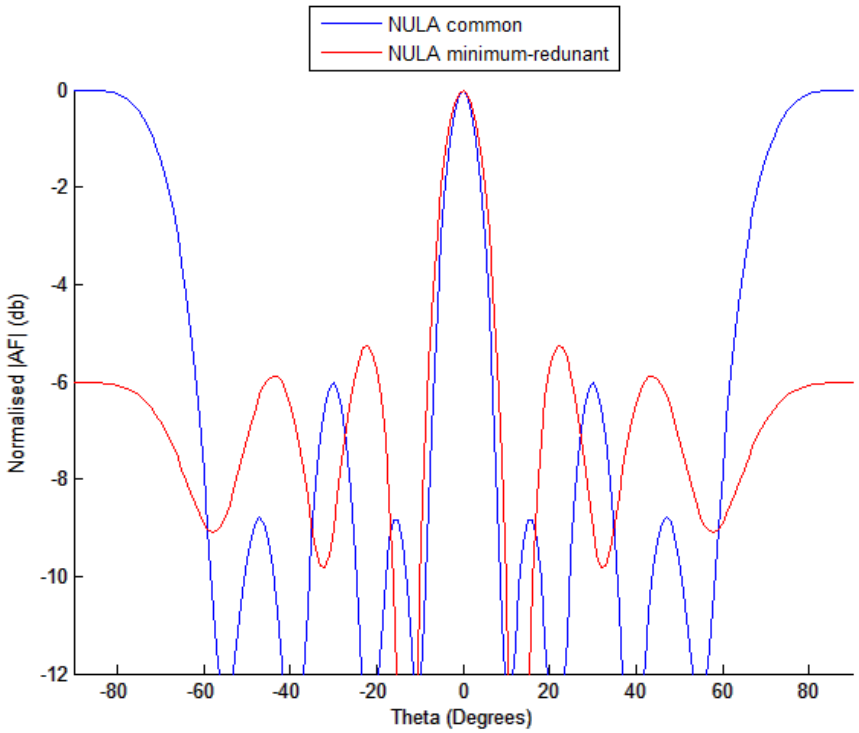

Figure 8: Radiation pattern of $N = 4$ common non-uniform linear array and its minimum-redundancy array counterpart.

performance provided by the minimum-redundancy array is less than desirable for our application.

5.1.2 Windowing functions

As discussed in Section 2, applying a weighting method to the signals received by each element is an effective means of distinguishing the mainlobe in the radiation pattern. This technique was explored by Noordin et al. and Sarker et al., who both determined that the Blackman window was the most effective in suppressing the outer sidelobes. To investigate these effects and whether there is an improvement in the estimation performance of the array, the Blackman window, whose equation is shown below, was used to filter various radiation patterns.

$$w(n) = a_0 - a_1 \cos\left(\frac{2\pi n}{N-1}\right) + a_2 \cos\left(\frac{4\pi n}{N-1}\right)$$

where:

- $\alpha = 0.16$
- $a_0 = \dfrac{1-\alpha}{2}$
- $a_1 = \dfrac{1}{2}$
- $a_2 = \dfrac{\alpha}{2}$

Figure 9 depicts the effects of subjecting the radiation pattern obtained from the 17-element uniform linear array from above to the Blackman window. It can be seen that as the phase increases, the sidelobe levels continually decrease, with the grating lobes inherent in the outer elements being heavily suppressed.

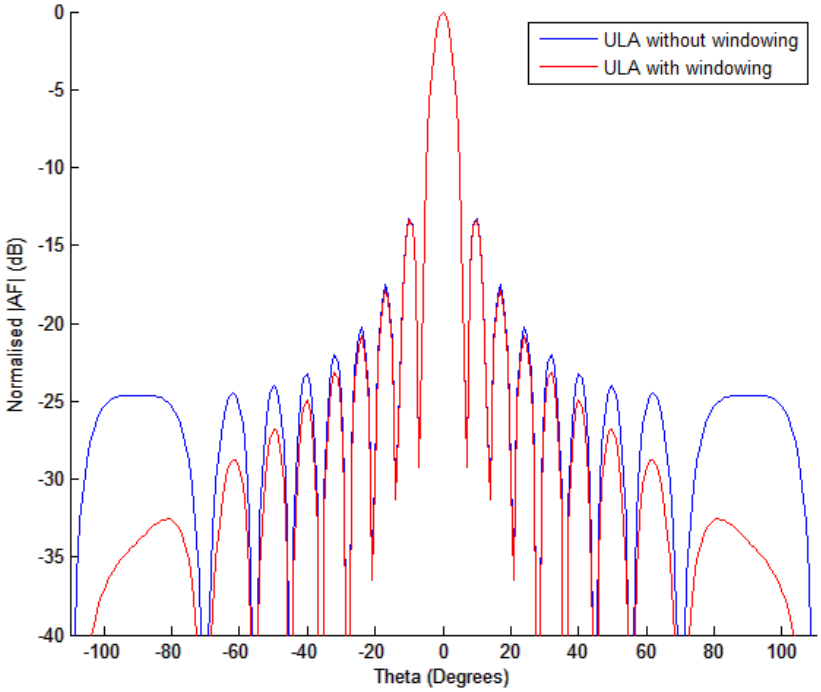

Figure 9: Blackman windowing used on the previous $N = 17$ element uniform linear array.

Our initial investigation into the Blackman windowing function lends credibility to Noordin et al. and Sarker et al.'s results. The windowing function is able to successfully suppress sidelobe levels, reducing inefficiencies in the array and allowing the mainlobe to be better distinguished. From the results obtained in Figure 9, it is logical that the inclusion of some form of windowing function is a necessity for the proposed solution.

It may be beneficial however, to investigate whether the windowing function itself can be assigned an optimal weighting. In this way, the positions of the elements may also be optimised according to this windowing function.

Manipulating the response of the array in this manner, in conjunction with assigning the SCC a specific masking value, should minimise inefficiencies in the array in accordance to the optimisation algorithms discussed in the following subsections. The inclusion of the windowing function into the optimisation process will be further discussed in Section 5.2.3.

5.2 Formulating the problem

To begin the development of the mathematical model surrounding the CRB and the SCC, we consider an initially uniform linear array consisting of N elements positioned along the x-axis of the Cartesian plane. We then have the following vectors described by the element positions,

$$\boldsymbol{x} = \begin{pmatrix} x_1 & ... & x_N \end{pmatrix}^{\mathrm{T}}, \boldsymbol{x}_{\boldsymbol{x}} = \begin{pmatrix} x_1^2 & ... & x_N^2 \end{pmatrix}^{\mathrm{T}} \tag{8}$$

For later calculations, it is convenient to form an expression for the array's centre of gravity, x_c, which we define as,

$$x_c = \frac{1}{N} \sum_{i=1}^{N} x_i \tag{9}$$

We then consider a narrow-band signal $s(t)$ with wavelength λ impinging on the array with azimuth angle ranging from $\phi_s \in [0, 2\pi]$. To simplify the calculations and optimisation process for this problem, we restrict the signal to propagate in only one dimension; possessing no elevation component. The steering vector of the signal is then defined by,

$$\boldsymbol{a} = \begin{pmatrix} e^{jk_0 x_1 u_s} & ... & e^{jk_0 x_N u_s} \end{pmatrix}^{\mathrm{T}} \tag{10}$$

where $k_0 = 2\pi/\lambda$ denotes the spatial frequency of the desired signal and $u_s = \sin\phi_s$ its direction vector component. With the assumption of omni-directional antennas and far-field sources, we can then express the received signal as,

$$X(t) = \boldsymbol{a}s(t) + \boldsymbol{n}(t),\ t = 1, .., T \tag{11}$$

which can be considered both deterministic and random if $s(t)$ itself is an unknown, deterministic and random signal, with $\boldsymbol{n}(t)$ denoting a stray signal interfering with the reception of $s(t)$. We continue with the assumptions that the estimated signal and interference are Gaussian in nature with zero mean, having constant variances σ_s^2 and σ_n^2 respectively. We may then define the signal-to-noise ratio to be $\rho = \dfrac{\sigma_s^2}{\sigma_n^2}$. Using these definitions, we then continue with the formulation of the CRB and SCC.

5.2.1 Cramér-Rao bound

In accordance with our first aim for this problem, the optimisation of the element positioning must be obtained through a determination of the CRB. Throughout the literature, the configuration of the elements within the array is often considered to be a continuous or discrete problem; the elements able to adopt any position

along a particular axis in the continuous case, or only allowed to assume specific locations in the discrete, with the elements being switched on or off. A distinction must be made in this case, as the formulation of the CRB differs in the continuous and discrete forms. Given that for our problem, the initial array is to have its elements repositioned along the x-axis, the decision was made for the configuration to be continuous in nature.

In order to determine the CRB, we must first find an expression for the Fisher information. We let the Fisher information for the estimation of azimuth angle ϕ_s be denoted by J. As derived previously in [21], [22] and [23], the CRB is a function of the array configuration whose parameter involves the element positions,

$$Q_{xx} = \sum_{i=1}^{N} (x_i - x_c)^2$$

As the array is symmetric about the origin, we have the centre of gravity of the array also residing at the origin, such that $x_c = 0$. We can then formulate the above as,

$$Q_{xx} = \sum_{i=1}^{N} x_i^2$$

This leaves us with a final expression for the parameter of the array configuration,

$$Q_{xx} = \mathbf{1}^{\mathrm{T}} \boldsymbol{x}_{\boldsymbol{x}} \tag{12}$$

where $\mathbf{1}^{\mathrm{T}}$ is a vertical vector of 1's, with Equation 12 denoting the squared summation of the element positions. From [21], [22] and [23], the Fisher information $\mathcal{J}$ of the estimated azimuth angle can then be expressed using this parameter, such that,

$$\mathcal{J} = \mathcal{G} \sin^2 \phi_s Q_{xx} \tag{13}$$

where $\mathcal{G} = 2N\rho^2 k_0^2/(1 + \rho N)$ is angle independent.

Having determined an expression for the Fisher information, we now formulate the CRB function as the inverse of the Fisher information,

$$\mathcal{C} = \mathcal{J}^{-1} = \frac{1}{\mathcal{G} \sin^2 \phi_s Q_{xx}} \tag{14}$$

In (14), we see that the CRB is described by the inverse of the configuration parameter Q_{xx}, with $\mathcal{G}$ and $\sin^2 \phi_s$ being constant values. We may therefore conclude that minimising the CRB function, $\mathcal{C}$, is equivalent to maximising the configuration parameter, Q_{xx}. As such, we may state the minimisation of the CRB as,

$$\min_{x_i} \quad \frac{1}{\sum_{i=1}^{N} x_i^2} \quad \leftrightarrow \quad \max_{x_i} \quad \sum_{i=1}^{N} x_i^2 \quad i = 1, \ldots, N \tag{15}$$

It is evident from (15) that in order to maximise the configuration parameter Q_{xx}, we must place the elements as far as possible from the centre of gravity of the array, i.e. at the very edges of the aperture. While this indeed minimises $\mathcal{C}$, this optimisation does not produce an ideal response from the array in terms of signal separability. While the positions of the elements have been 'optimised', the trivial nature of this optimisation process renders the minimisation as ineffective in the context of extrapolating relevant information from a signal being interfered with. In this regard, we impose the SCC as a form of constraint on the optimisation of $\mathcal{C}$ in order to improve the response of the array and to allow for the rejection of interfering signals. We see in the following section the derivation of the SCC and its relation as a constraint on the CRB function.

5.2.2 Spatial Correlation Coefficient

The impact of interference on the desired signal is one that is characterised by the performance of the array in the form of its radiation pattern. It has been shown that the configuration of the array is not only fundamental to its estimation performance, but also in its ability to separate multiple signals from one another within an environment rich in EM energy. In following the second aim of this problem, an expression for the SCC must be determined so as to develop a constraint on the CRB function derived previously. In this way, a joint cost function of the CRB and SCC can be developed that allows for the element positions to be optimised in such a manner that the estimation performance and interference rejection are optimally balanced.

To begin the derivation of the SCC, we define the following vectors,

$$\boldsymbol{v_s} = \begin{pmatrix} v_s(1) \\ \vdots \\ v_s(N) \end{pmatrix}, \boldsymbol{v_j} = \begin{pmatrix} v_j(1) \\ \vdots \\ v_j(N) \end{pmatrix} \tag{16}$$

where $v_s(i) = e^{jk_o x_i u_s}$ and $v_j(i) = e^{jk_o x_i u_j}$ for $i = 1, ..., N$, and $u_i = \sin\phi_i$ for $i = s, j$ representing the direction vector component for the desired and interference signals respectively.

Since the SCC denotes the cross correlation between the steering vectors of two separated incoming sources, it is only dependent on electrical angle differences. It can be seen in Figure 10 that the SCC can be described by the cosine of the angle θ between the desired signal and the interference, as the SCC determines the orthogonality between two subspaces. We then define the SCC as:

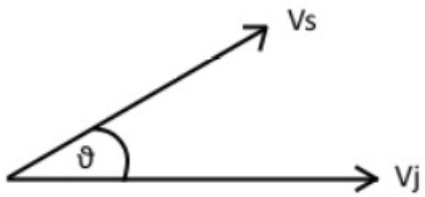

Figure 10: Relationship between the signal $\boldsymbol{v_s}$ and interference $\boldsymbol{v_j}$ vectors.

$$\alpha_{js} = \cos\theta = \frac{\boldsymbol{v}_j^{\mathrm{H}}\boldsymbol{v}_s}{\boldsymbol{v}_j\boldsymbol{v}_s} = \frac{\boldsymbol{v}_j^{\mathrm{H}}\boldsymbol{v}_s}{\sqrt{\boldsymbol{v}_j^{\mathrm{H}}\boldsymbol{v_s}}\sqrt{\boldsymbol{v}_j\boldsymbol{v}_s}} = \frac{\boldsymbol{v}_j^{\mathrm{H}}\boldsymbol{v}_s}{N} \tag{17}$$

We may thus express the SCC in the form,

$$|\alpha_{js}| = \frac{|\mathbf{1}^{\mathrm{T}}\boldsymbol{v_{js}}|}{N} \Leftrightarrow |\alpha_{js}|^2 = \frac{\mathbf{1}^{\mathrm{T}}\boldsymbol{W_r}\mathbf{1}}{N^2} \tag{18}$$

where $\boldsymbol{W_r} = \Re(\boldsymbol{v_{js}}\boldsymbol{v_{js}}^{\mathrm{H}})$ and $\boldsymbol{v_{js}}$ is the corresponding steering vector defined as the Hadamard product between the desired and interfering signals, such that:

$$\begin{aligned}\boldsymbol{v_{js}} &= \boldsymbol{v_s} \circ \boldsymbol{v_j^*} \\ &= e^{jk_0x_i(u_s-u_j)} \text{ for } i = 1, ..., N\end{aligned}$$

With this expression of the SCC, the assignment of a masking value, as described in Section 4.3, allows for the regulation of sidelobe levels by permitting them to reach a maximum magnitude. To assign the maximum value of the SCC over a range of angles, we may formulate the constraint as,

$$|\alpha_{js}|^2 = \frac{\mathbf{1}^{\mathrm{T}}\boldsymbol{W_r}\mathbf{1}}{N^2} = c \tag{19}$$

Having now determined a suitable expression for the SCC, the following subsection details the construction of the windowing function utilised in the solution to this study.

5.2.3 Manual Windowing Function

As shown in Section 5.1.2, the application of a windowing function improves the regulation of sidelobe levels and contributes towards distinguishing the mainlobe within the radiation pattern. Due to the few number of elements that will be used in the implementation of this low-cost system, the sidelobes towards the aperture of the array will need to be suppressed. To accommodate for the array's beam steering angle from $[-\pi/2, \pi/2]$,

we construct our windowing function using seven coefficients to cover the array's azimuth, symbolised by the following vector,

$$\boldsymbol{\delta} = \begin{bmatrix} 0.001 & 0.01 & 0.1 & 1 & 0.1 & 0.01 & 0.001 \end{bmatrix} \tag{20}$$

The vector described in (20) corresponds to an array with its steering angle positioned at 0°. As the array is steered to point in other directions, the coefficients of the windowing function must be accordingly repositioned within the vector such that $\delta_i = 1$ is aligned with that particular steering angle, where i denotes the index of the vector corresponding to the entry '1'. In this way, we are able to ensure that the radiation pattern does not exceed a specific normalised value within the azimuth range of $[-\pi/2, \pi/2]$. We hence define the windowing function as,

$$h_m(\boldsymbol{x}) = \delta_m, \text{ for } m = 1, \ldots, k \tag{21}$$

where $h_m(\boldsymbol{x}) = \dfrac{1}{N}\left|\sum_{i=1}^{N} e^{jk_0 x_i u_i}\right|$ formally defines the absolute value of the array factor.

The manual windowing function was deemed a more optimal choice over the Blackman window investigated in Section 5.1 due to the ability to optimise for its weighting within the expression of the Lagrange function. As will be shown in the following subsection, by determining the optimal Lagrange multiplier for the associated windowing function, we may combine the optimisation of the windowing function with the constraints of the SCC and the CRB. In this way, we can balance the regulation of these sidelobe levels with the estimation performance and rejection criteria, instead of utilising otherwise inflexible windowing methods.

5.2.4 Establishing the Lagrange Function

Having determined expressions for the CRB, SCC and the manual windowing function, a model for the mathematical optimisation can now be formed. For this problem, we intend to minimise the CRB using the SCC and the manual windowing function as constraints, allowing us to achieve the optimum balance between estimation performance and the separation of incoming signals, while manually suppressing sidelobe levels in the array's response.

Using (15), (19) and (21), we are thus able to state the optimisation as a minimisation problem in the form,

$$\begin{aligned} \min_{x_i} \quad & \frac{1}{\sum_{i=1}^{N} x_i^2} && i = 1, \ldots, N \\ \text{s.t.} \quad & \frac{\mathbf{1}^{\mathrm{T}} \boldsymbol{W_r} \mathbf{1}}{N^2} = c, \quad \frac{1}{N}\left|\sum_{i=1}^{N} e^{jk_0 x_i u_i}\right| = \delta_m \end{aligned} \tag{22}$$

The model formulated above functions as a mathematical expression of the objectives described in Section 3.

With this expression, it is necessary to evaluate its terms and to determine a solution to a particular input stimulus using the method of trust-regions as discussed in Section 4.5. To do this, we establish the Lagrange function as mentioned previously using (22).

Following the process outlined in Section 4.4, with the function to be minimised in (22) being the CRB, we assign the Lagrange multipliers λ_0 and λ_m to the SCC and manual windowing functions respectively. Using the form described in (6), we construct the following Lagrange function for the optimisation problem,

$$\mathcal{L}(\boldsymbol{x}, \boldsymbol{\lambda}) = \frac{1}{\sum_{i=1}^{N} x_i^2} + \lambda_0 \left(\frac{\mathbf{1}^{\mathrm{T}} \boldsymbol{W_r} \mathbf{1}}{N^2} - c \right) + \sum_{m=1}^{k} \lambda_m \left(\frac{1}{N} \left| \sum_{i=1}^{N} e^{jk_0 x_i u_i} \right| - \delta_m \right) \tag{23}$$

where $\mathcal{L}$ is a function of $\boldsymbol{x}$ and $\boldsymbol{\lambda}$, with $\boldsymbol{x}$ denoting the vector of element positions in the array and $\boldsymbol{\lambda}$ the vector of Lagrange multipliers. To continue the optimisation process involving the Lagrange function, we first evaluate the SCC term inside (23) using the definitions from (18). Expanding $\boldsymbol{W_r}$ and solving for $\boldsymbol{v_{js}} \boldsymbol{v_{js}}^{\mathrm{H}}$, we have,

$$\boldsymbol{v_{js}} \boldsymbol{v_{js}}^{\mathrm{H}} = \begin{pmatrix} e^{jk_0 x_1 (u_s - u_j)} \\ \vdots \\ e^{jk_0 x_N (u_s - u_j)} \end{pmatrix} \begin{pmatrix} e^{-jk_0 x_1 (u_s - u_j)} & \dots & e^{-jk_0 x_N (u_s - u_j)} \end{pmatrix} \tag{24}$$

$$= \begin{pmatrix} 1 & e^{jk_0 (u_s - u_j)(x_1 - x_2)} & e^{jk_0 (u_s - u_j)(x_1 - x_3)} & \dots & e^{jk_0 (u_s - u_j)(x_1 - x_N)} \\ e^{-jk_0 (u_s - u_j)(x_1 - x_2)} & 1 & e^{jk_0 (u_s - u_j)(x_2 - x_3)} & \dots & e^{jk_0 (u_s - u_j)(x_2 - x_N)} \\ e^{-jk_0 (u_s - u_j)(x_1 - x_3)} & e^{-jk_0 (u_s - u_j)(x_2 - x_3)} & 1 & \dots & e^{jk_0 (u_s - u_j)(x_3 - x_N)} \\ \vdots & \vdots & \vdots & \vdots & \vdots \\ e^{-jk_0 (u_s - u_j)(x_1 - x_N)} & e^{-jk_0 (u_s - u_j)(x_2 - x_N)} & e^{-jk_0 (u_s - u_j)(x_3 - x_N)} & \dots & 1 \end{pmatrix} \tag{25}$$

Taking the real component of the above, we find that,

$$\Re \left(\boldsymbol{v_{js}} \boldsymbol{v_{js}}^{\mathrm{H}} \right) = \begin{pmatrix} 1 & \cos(\beta(x_1 - x_2)) & \cos(\beta(x_1 - x_3)) & \dots & \cos(\beta(x_1 - x_N)) \\ \cos(\beta(x_1 - x_2)) & 1 & \cos(\beta(x_2 - x_3)) & \dots & \cos(\beta(x_2 - x_N)) \\ \cos(\beta(x_1 - x_3)) & \cos(\beta(x_2 - x_3)) & 1 & \dots & \cos(\beta(x_3 - x_N)) \\ \vdots & \vdots & \vdots & \vdots & \vdots \\ \cos(\beta(x_1 - x_N)) & \cos(\beta(x_2 - x_N)) & \cos(\beta(x_3 - x_N)) & \dots & 1 \end{pmatrix} \tag{26}$$

where $\beta = k_0(u_s - u_j)$. Using (26), we can now fully evaluate the expression of the SCC in (23), such that,

$$\mathbf{1}^{\mathrm{T}} \boldsymbol{W_r} \mathbf{1} = \mathbf{1}^{\mathrm{T}} \Re \left(\boldsymbol{v_{js}} \boldsymbol{v_{js}}^{\mathrm{H}} \right) \mathbf{1} = \sum_{m=1}^{N} \cos(\beta(x_i - x_m)), \text{ for } i = 1 \dots N \tag{27}$$

With this expansion of the SCC term, we can now rewrite (23) in terms of the variables x_i and the Lagrange

multipliers so as to construct a set of equations using partial differentiation techniques as outlined in Section 4.4. We therefore rewrite (23) as,

$$\therefore \mathcal{L}(\boldsymbol{x}, \boldsymbol{\lambda}) = \frac{1}{\sum_{i=1}^{N} x_i^2} + \lambda_0 \left(\frac{1}{N^2} \sum_{m=1}^{N} \cos(\beta(x_i - x_m)) - c \right) + \sum_{m=1}^{k} \lambda_m \left(\frac{1}{N} \left| \sum_{i=1}^{N} e^{jk_0 x_i u_i} \right| - \delta_m \right) \tag{28}$$

To obtain this set of equations, we partially differentiate (28) with respect to the position variable x_i and the Lagrange multipliers associated with the SCC and manual windowing function terms. Beginning with the position variable, we have the following partial differentiation,

$$\frac{\delta}{\delta x_i} \left(\mathcal{L}\left(\boldsymbol{x}, \boldsymbol{\lambda}\right) \right) = \frac{\delta}{\delta x_i} \left(\frac{1}{\sum_{i=1}^{N} x_i^2} \right) + \frac{\delta}{\delta x_i} \left(\lambda_0 \left(\frac{1}{N^2} \sum_{m=1}^{N} \cos(\beta(x_i - x_m)) - c \right) \right) + \frac{\delta}{\delta x_i} \left(\sum_{m=1}^{k} \lambda_m \left(\frac{1}{N} \left| \sum_{i=1}^{N} e^{jk_0 x_i u_i} \right| - \delta_m \right) \right)$$

$$\therefore \frac{\delta}{\delta x_i} \left(\mathcal{L}\left(\boldsymbol{x}, \boldsymbol{\lambda}\right) \right) = \frac{-2x_i}{\left(\sum_{i=1}^{N} x_i^2 \right)^2} - \lambda_0 \frac{1}{N^2} \beta \sum_{m=1}^{N} \sin(\beta(x_i - x_m)) \tag{29}$$

Continuing with the first Lagrange multiplier, λ_0, for the SCC component in (28), we have,

$$\frac{\delta}{\delta \lambda_0} \left(\mathcal{L}\left(\boldsymbol{x}, \boldsymbol{\lambda}\right) \right) = \frac{\delta}{\delta \lambda_0} \left(\frac{1}{\sum_{i=1}^{N} x_i^2} \right) + \frac{\delta}{\delta \lambda_0} \left(\lambda_0 \left(\frac{1}{N^2} \sum_{m=1}^{N} \cos(\beta(x_i - x_m)) - c \right) \right) + \frac{\delta}{\delta \lambda_0} \left(\sum_{m=1}^{k} \lambda_m \left(\frac{1}{N} \left| \sum_{i=1}^{N} e^{jk_0 x_i u_i} \right| - \delta_m \right) \right)$$

$$\therefore \frac{\delta}{\delta \lambda_0} \left(\mathcal{L}\left(\boldsymbol{x}, \boldsymbol{\lambda}\right) \right) = \frac{1}{N^2} \sum_{m=1}^{N} \cos(\beta(x_i - x_m)) - c \tag{30}$$

For the final Lagrange multiplier, λ_m, for the manual windowing component in (28), we have,

$$\frac{\delta}{\delta \lambda_m} \left(\mathcal{L}\left(\boldsymbol{x}, \boldsymbol{\lambda}\right) \right) = \frac{\delta}{\delta \lambda_m} \left(\frac{1}{\sum_{i=1}^{N} x_i^2} \right) + \frac{\delta}{\delta \lambda_m} \left(\lambda_0 \left(\frac{1}{N^2} \sum_{m=1}^{N} \cos(\beta(x_i - x_m)) - c \right) \right) + \frac{\delta}{\delta \lambda_m} \left(\sum_{m=1}^{k} \lambda_m \left(\frac{1}{N} \left| \sum_{i=1}^{N} e^{jk_0 x_i u_i} \right| - \delta_m \right) \right)$$

$$\therefore \frac{\delta}{\delta \lambda_m} \left(\mathcal{L}\left(\boldsymbol{x}, \boldsymbol{\lambda}\right) \right) = \sum_{m=1}^{k} \left(\frac{1}{N} \left| \sum_{i=1}^{N} e^{jk_0 x_i u_i} \right| - \delta_m \right) \tag{31}$$

With these partially differentiated functions, we may now formulate the equation set derived from the Lagrange function. Reiterating the results from the above calculations, we have,

$$\begin{cases} \dfrac{\delta}{\delta x_i}\left(\mathcal{L}\left(\boldsymbol{x},\boldsymbol{\lambda}\right)\right) = \dfrac{-2x_i}{\left(\sum_{i=1}^{N} x_i^2\right)^2} - \dfrac{\lambda_0}{N^2}\beta\sum_{m=1}^{N}\sin(\beta(x_i - x_m)) \\ \dfrac{\delta}{\delta \lambda_0}\left(\mathcal{L}\left(\boldsymbol{x},\boldsymbol{\lambda}\right)\right) = \dfrac{1}{N^2}\sum_{m=1}^{N}\cos(\beta(x_i - x_m)) - c \\ \dfrac{\delta}{\delta \lambda_m}\left(\mathcal{L}\left(\boldsymbol{x},\boldsymbol{\lambda}\right)\right) = \sum_{m=1}^{k}\left(\dfrac{1}{N}\left|\sum_{i=1}^{N} e^{jk_0 x_i u_i}\right| - \delta_m\right) \end{cases}$$

As mentioned in Section 4.4, this set of equations is conventionally solved by analytically evaluating the partial derivatives and solving the unconstrained resulting equations. In this way, we should be able to determine the optimal solutions for the variables x_i and $\boldsymbol{\lambda}$. In our case however, we face the issue where our set of equations are non-linear, rendering any form of analytical evaluation much more complex. Additionally, given the number of variables, this conventional form of evaluation would prove arduous to complete. To resolve this issue, we instead adopt a form of numerical analysis that will be detailed in the following section.

5.2.5 Simulation of Cost Function

In order to derive a set of solutions from this optimisation process, we solve the set of non-linear equations derived in Section 5.2.4 using numerical methods. As mentioned above, the analytical method of determining the optimum values for x_i and $\boldsymbol{\lambda}$ proves vastly complex, with the number of variables changing depending on the number of windowing coefficients being used. To solve this set of equations, we employ the use of MATLAB to efficiently simulate an optimum solution set.

As described in Section 4.5, the method of trust-region analysis was used in conjunction with the fsolve function in MATLAB to numerically solve the Lagrange function. To implement this, three core scripts were created within MATLAB, whose code can be reviewed in the appendices: 'dfunc.m', 'func.m' and 'opt_test.m'.

The MATLAB script, dfunc.m, functions as a method of numerically approximating the partial derivatives calculated in Section 5.2.4. It was shown previously in Section 4.4 that the minima and maxima of the Lagrange function are located where its partial derivatives are equal to zero, i.e. when $\dfrac{\delta}{\delta x_i}\left(\mathcal{L}\left(\boldsymbol{x},\boldsymbol{\lambda}\right)\right) = 0$, $\dfrac{\delta}{\delta \lambda_0}\left(\mathcal{L}\left(\boldsymbol{x},\boldsymbol{\lambda}\right)\right) = 0$ and $\dfrac{\delta}{\delta \lambda_m}\left(\mathcal{L}\left(\boldsymbol{x},\boldsymbol{\lambda}\right)\right) = 0$. With this knowledge, the function takes in a vector describing the position of the elements in the array, $\boldsymbol{x}$, and computes the partial derivatives of the function at the point described by that vector. By taking incremental steps, the function uses a central finite difference approach in its computation of $\dfrac{\delta}{\delta x_i}\left(\mathcal{L}\left(\boldsymbol{x},\boldsymbol{\lambda}\right)\right)$, $\dfrac{\delta}{\delta \lambda_0}\left(\mathcal{L}\left(\boldsymbol{x},\boldsymbol{\lambda}\right)\right)$ and $\dfrac{\delta}{\delta \lambda_m}\left(\mathcal{L}\left(\boldsymbol{x},\boldsymbol{\lambda}\right)\right)$ in each iteration.

Complementing this script, func.m returns the value of the Lagrange function at the point described by the input vector $\boldsymbol{x}$. Here, the particular DoA of the desired and interfering signals are defined, as well as the

coefficients of the manual windowing function. By evaluating the values of the array factor as described by (21), these values are then incorporated into the Lagrange function, shown in (28), along with the CRB and SCC.

The file opt_test.m operates as a wrapper function that combines func.m and dfunc.m. By using the fsolve function in MATLAB, the method of trust-region analysis is used iteratively to determine the maximum or minimum values of the Lagrange function within a neighbourhood. In this way, as dfunc.m returns two solutions corresponding to either the minimum or maximum, we take the global minimum of the solution set returned within the neighbourhood. This global minimum is then the most optimised solution in accordance to the imposed constraints.

The implementation of these files within the simulation environment follows an iterative process enumerated below:

1. Begin with a uniform linear array.
2. Pass vector of element positions into the Lagrange function.
3. Record value of cost function.
4. Increment element positions by pre-defined step size.
5. Determine value of cost function at new position.
6. If value from step 5 is smaller than value from step 3, repeat process from step 3.

In the case where the value of the cost function determined in step 5 is not smaller than step 3, the neighbourhood N is adjusted and the process restarted.

This section has described the theoretical methodology adopted for determining the mathematical model and the means with which to simulate it. The MATLAB code for each of the functions described above, as well as all peripheral code, can be found in Appendices B. The following section details the theoretical results obtained by implementing these algorithms and using these MATLAB scripts.

6 Results

In order to completely model the functionalities of the optimised method, the versatility of the array and its ability to form a trade-off between estimation performance, signal separability and sidelobe level regulation was tested. As such, the simulation of the mathematical model was comprised of two scenarios: when the desired signal impinged directly on the array and when it impinged at an oblique angle. This way, we could test how the array would respond when needing to be steered to other directions and whether this would affect its ability to determine the final, optimised element placements for a particular DoA of the desired and interfering signal. Within each scenario, to test the trade-off between estimation performance and signal separability, differing values of the SCC value, c, were simulated and used to gauge whether the optimised array exhibited improved performance over its uniform counterpart.

6.1 Direct Impingement

We begin the simulation with the first scenario, starting with a uniform linear array symmetric about the origin consisting of $N = 5$ elements, with inter-element spacing of $\lambda/2$, where λ is the wavelength of the desired signal. We set the frequency of the signal to 0.3 GHz, with our windowing function being comprised of $k = 7$ coefficients. The angle of arrival of the desired signal was set to 0° and the interfering signal set to 30°. The results obtained from this first scenario are depicted in the following figures. Additionally, the resulting 3D depictions of the trust-regions for each value of c in this scenario can be found in Appendices A.

6.1.1 Simulation 1: $c = 0$

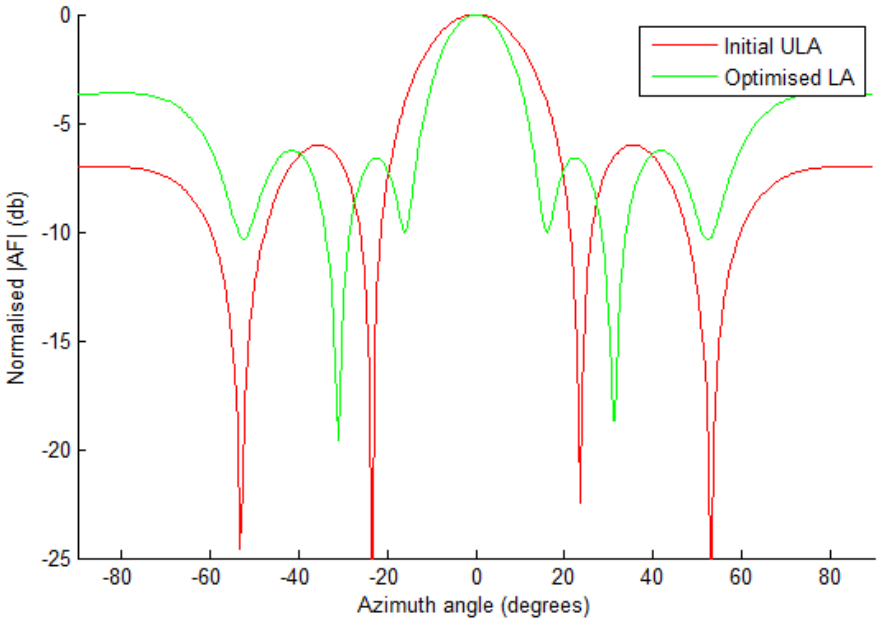

Figure 11: Radiation pattern comparing the uniform linear array and the optimised linear array, with $c = 0$.

Array	1	2	3	4	5
Initial ULA (m)	-1	-0.5	0	0.5	1
Optimised LA (m)	-1.5725	-0.9040	-0.2692	0.4525	1.4015

Table 1: Comparison of element positioning between the unoptimised array and the optimised linear array with $c = 0$.

From Figure 11, we make the following comparison shown in Table 2 between the unoptimised and optimised arrays regarding their first sidelobe level, aperture length and half-power beamwidth.

Characteristic	Initial ULA	Optimised LA
First SLL (dB)	-6.021	-6.596
Aperture length (m)	2	2.974
Half-power beamwidth (degrees)	28.65	19.481

Table 2: Comparison of characteristics between the unoptimised uniform and optimised linear array with $c = 0$.

6.1.2 Simulation 2: $c = 0.02$

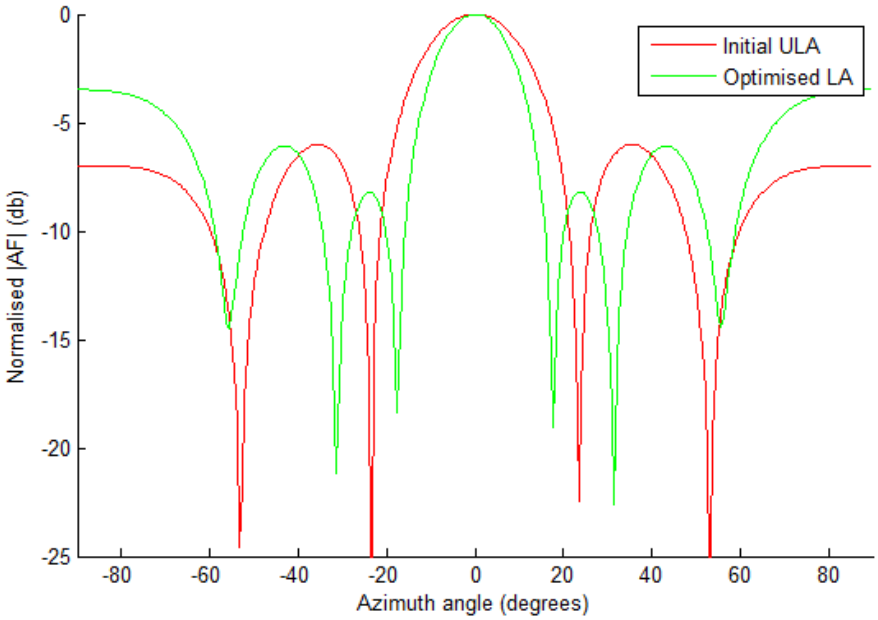

Figure 12: Radiation pattern comparing the uniform linear array and the optimised linear array, with $c = 0.02$.

Array	1	2	3	4	5
Initial ULA (m)	-1	-0.5	0	0.5	1
Optimised LA (m)	-2.0822	-1.2555	-0.6570	-0.0366	0.7437

Table 3: Comparison of element positioning between the unoptimised array and the optimised linear array with $c = 0.02$.

Characteristic	Initial ULA	Optimised LA
First SLL (dB)	-6.021	-8.196
Aperture length (m)	2	2.8259
Half-power beamwidth (degrees)	28.65	20.72

Table 4: Comparison of characteristics between the unoptimised uniform and optimised linear array with $c = 0.02$.

6.1.3 Simulation 3: $c = 0.04$

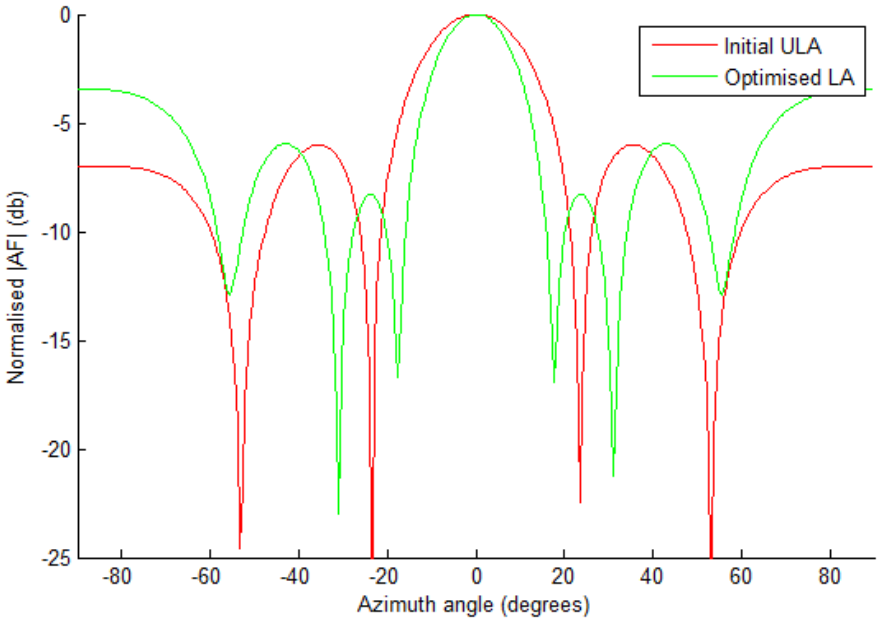

Figure 13: Radiation pattern comparing the uniform linear array and the optimised linear array, with $c = 0.04$.

Array	1	2	3	4	5
Initial ULA (m)	-1	-0.5	0	0.5	1
Optimised LA (m)	-2.2858	-1.4395	-0.8462	-0.2265	0.5470

Table 5: Comparison of element positioning between the unoptimised array and the optimised linear array with $c = 0.04$.

Characteristic	Initial ULA	Optimised LA
First SLL (dB)	-6.021	-8.3
Aperture length (m)	2	2.8328
Half-power beamwidth (degrees)	28.65	20.64

Table 6: Comparison of characteristics between the unoptimised uniform and optimised linear array with $c = 0.04$.

6.1.4 Simulation 4: $c = 0.08$

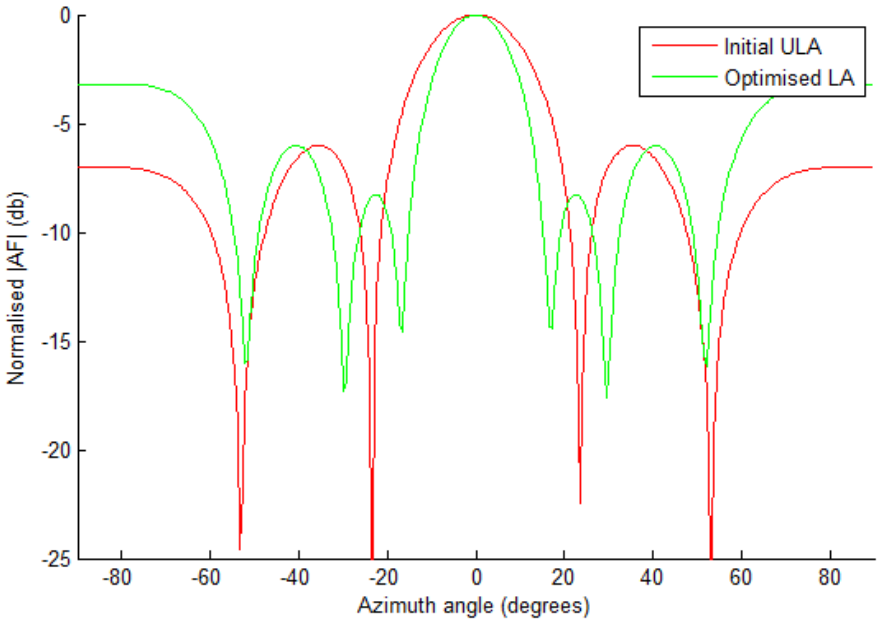

Figure 14: Radiation pattern comparing the uniform linear array and the optimised linear array, with $c = 0.08$.

Array	1	2	3	4	5
Initial ULA (m)	-1	-0.5	0	0.5	1
Optimised LA (m)	-11.3495	-10.5404	-9.9263	-9.2772	-8.3862

Table 7: Comparison of element positioning between the unoptimised array and the optimised linear array with $c = 0.08$.

Characteristic	Initial ULA	Optimised LA
First SLL (dB)	-6.021	-8.357
Aperture length (m)	2	2.9633
Half-power beamwidth (degrees)	28.65	19.572

Table 8: Comparison of characteristics between the unoptimised uniform and optimised linear array with $c = 0.08$.

6.2 Oblique Impingement

For the second scenario, in order to test the optimisation of the array when its beam had been steered, the DoA of the desired and interfering signal were altered such that $\phi_s = 30°$ and $\phi_n = 50°$. As the mainlobe was now being steered to a direction of 30°, the coefficients of the windowing function were correspondingly changed, with $\boldsymbol{\delta} = \begin{bmatrix} 0.01 & 0.001 & 0.01 & 0.1 & 1 & 0.1 & 0.01 \end{bmatrix}$. This way, the element $\delta_5 = 1$ allows for a maximum response in the radiation pattern at an angle of 30°, aligning with the quantisation of the azimuth angle $\phi \in [-\pi/2, \pi/2]$ into seven discrete levels. The results obtained from this second scenario are depicted in the following figures, with the 3D depictions of the trust-regions for the oblique impingement shown in Appendices A.

6.2.1 Simulation 1: $c = 0$

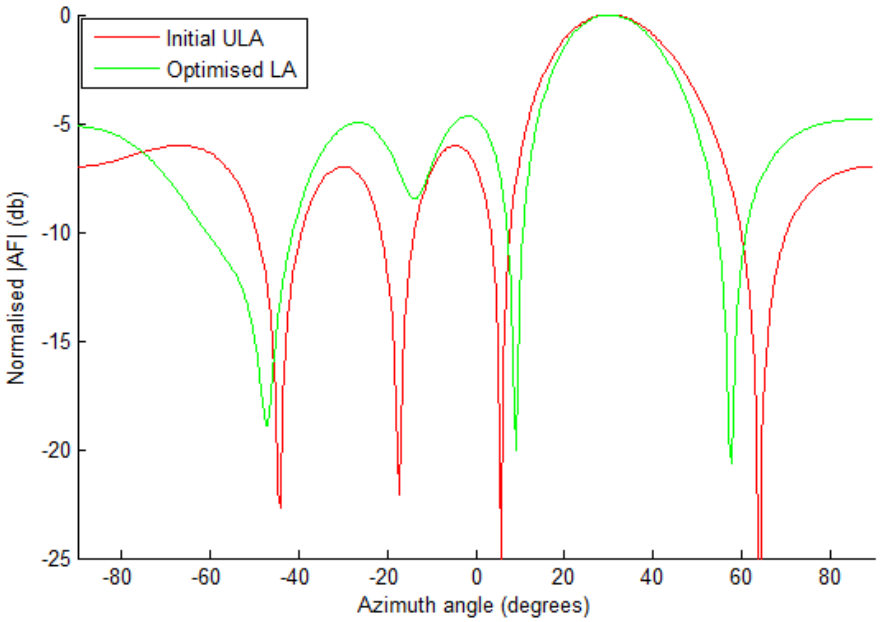

Figure 15: Radiation pattern comparing the uniform linear array and the optimised linear array, with $c = 0$.

Array	1	2	3	4	5
Initial ULA (m)	-1	-0.5	0	0.5	1
Optimised LA (m)	-1.0133	-0.6065	0.1063	0.6392	1.1826

Table 9: Comparison of element positioning between the unoptimised array and the optimised linear array with $c = 0$.

Characteristic	Initial ULA	Optimised LA
First SLL (dB)	-6.021	-4.664
Aperture length (m)	2	2.1959
Half-power beamwidth (degrees)	30.3	26.8

Table 10: Comparison of characteristics between the unoptimised uniform and optimised linear array with $c = 0$.

6.2.2 Simulation 2: $c = 0.02$

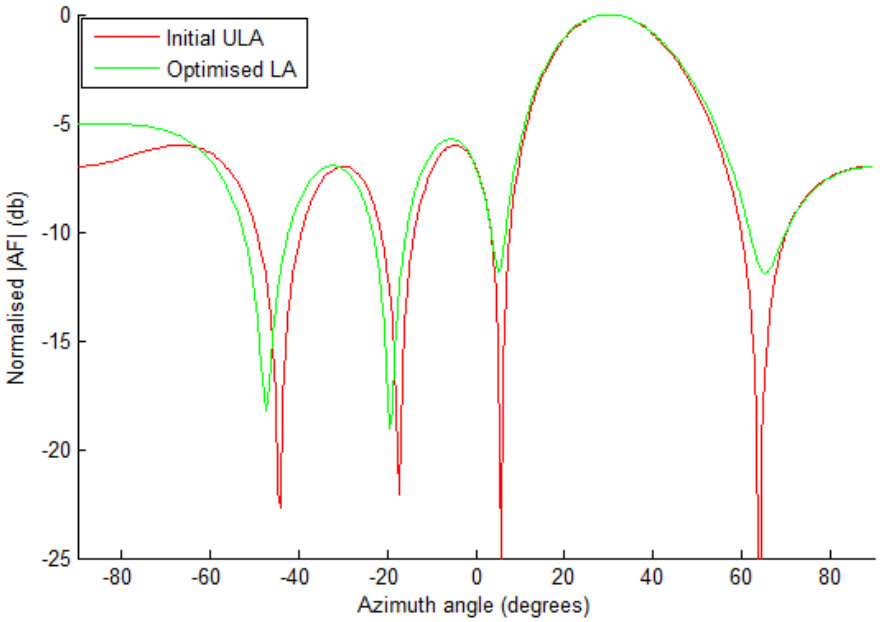

Figure 16: Radiation pattern comparing the uniform linear array and the optimised linear array, with $c = 0.02$.

Array	1	2	3	4	5
Initial ULA (m)	-1	-0.5	0	0.5	1
Optimised LA (m)	-0.9523	-0.5308	-0.0732	0.4441	0.9846

Table 11: Comparison of element positioning between the unoptimised array and the optimised linear array with $c = 0.02$.

Characteristic	Initial ULA	Optimised LA
First SLL (dB)	-6.021	-5.74
Aperture length (m)	2	1.9369
Half-power beamwidth (degrees)	30.3	31.44

Table 12: Comparison of characteristics between the unoptimised uniform and optimised linear array with $c = 0.02$.

6.2.3 Simulation 3: $c = 0.04$

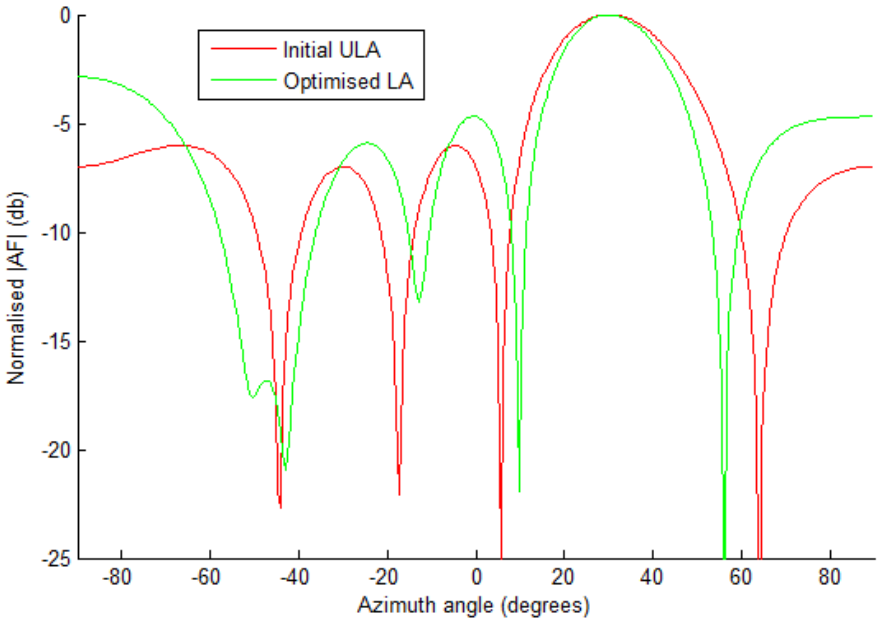

Figure 17: Radiation pattern comparing the uniform linear array and the optimised linear array, with $c = 0.04$.

Array	1	2	3	4	5
Initial ULA (m)	-1	-0.5	0	0.5	1
Optimised LA (m)	-1.0741	-0.5983	0.0830	0.7012	1.2205

Table 13: Comparison of element positioning between the unoptimised array and the optimised linear array with $c = 0.04$.

Characteristic	Initial ULA	Optimised LA
First SLL (dB)	-6.021	-4.706
Aperture length (m)	2	2.2946
Half-power beamwidth (degrees)	30.3	25.72

Table 14: Comparison of characteristics between the unoptimised uniform and optimised linear array with $c = 0.04$.

6.2.4 Simulation 4: $c = 0.08$

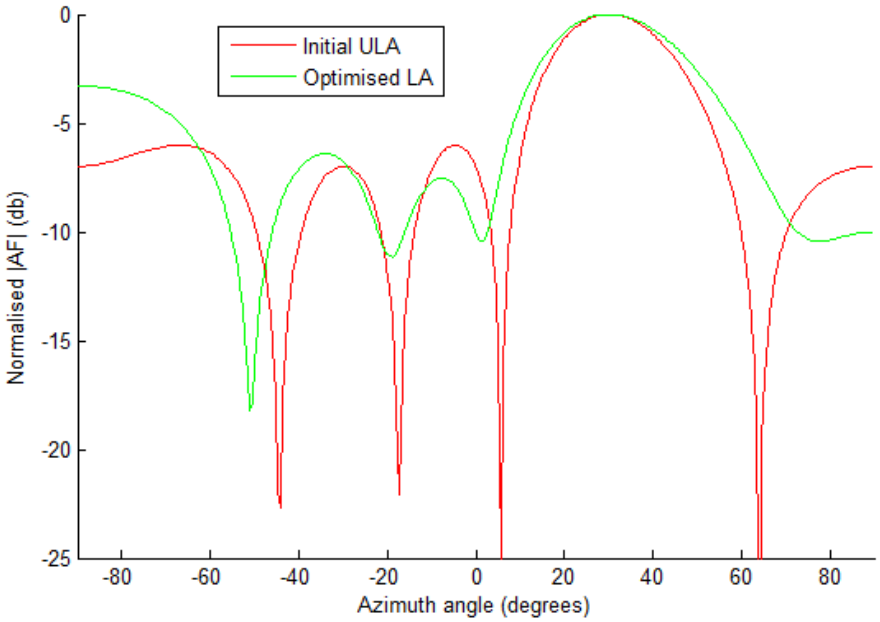

Figure 18: Radiation pattern comparing the uniform linear array and the optimised linear array, with $c = 0.08$.

Array	1	2	3	4	5
Initial ULA (m)	-1	-0.5	0	0.5	1
Optimised LA (m)	-0.8079	-0.3298	-0.02270	0.4177	0.9879

Table 15: Comparison of element positioning between the unoptimised array and the optimised linear array with $c = 0.08$.

Characteristic	Initial ULA	Optimised LA
First SLL (dB)	-6.021	-7.532
Aperture length (m)	2	1.7958
Half-power beamwidth (degrees)	30.3	34.88

Table 16: Comparison of characteristics between the unoptimised uniform and optimised linear array with $c = 0.08$.

Section 7 will discuss the results presented above, with a comparison being made to existing works that attempt to solve for a similar problem. This will then be followed by a discussion regarding the potential for future work.

7 Discussion/Evaluation

7.1 Direct Impingement

7.1.1 Simulation 1: $c = 0$

It is immediately noticeable in Figure 11 that the estimation performance of the system has been greatly improved over the initial configuration, with the optimised linear array possessing a much narrower mainlobe beamwidth. From Table 2, it can be calculated that there is a 32% reduction in the mainlobe beamwidth.

As $c = 0$, the regulation of sidelobe levels is not accounted for in the optimised system, with the position of the elements only optimising the estimation performance and separation of multiple signals. However, it can be seen that even with $c = 0$, the first sidelobe level of the optimised array is 0.575 dB lower than that of the initial array. Despite such a small value, the decrease in sidelobe level here lends credence to the performance of the optimisation algorithm. With the simulation using only $N = 5$ elements, it is natural for the sidelobe levels to behave undesirably. The suppression of the first sidelobe in this case is indicative of how much control we have over the radiation pattern as the value of c is altered.

At the azimuth angle of 30°, the null in the radiation pattern depicts the rejection of the interfering signal at its bearing. As the array is steered to 0°, the radiation pattern is reflected about this point, with a corresponding null being mirrored at −30°. This shows that the optimised system is able to separate the desired signal from the interference; a capability that the initial array was not able to provide.

The figures in Table 1 show that the element positions of the optimised array remain close to the initial element spacings, with no more than a maximum displacement of 0.572 metres from their initial positions. This implies that the configuration of the optimised array can be achieved by simply making minor adjustments to the initial positions. As such, the aperture length of the optimised array is 0.974 metres longer than the initial uniform linear array. This difference is very small in the context of the improvements made, with the length of the aperture remaining a sensible and practical size.

7.1.2 Simulation 2: $c = 0.02$

In Figure 12, the estimation performance is largely similar to that achieved in Simulation 1. The beamwidth of the mainlobe has increased by 1.239 dB from its previous value, rendering a 27.68% reduction in mainlobe beamwidth from the initial uniform linear array. Despite this reduction, the optimised array has still improved the estimation performance over the original system. It is possible that this reduction is due to the algorithm attempting to compromise between estimation performance and the regulation of sidelobe levels, as the value of c is no longer its ideal value of 0.

With $c = 0.02$, the regulation of sidelobe levels is now accounted for in the optimised system, with the first sidelobe level positioned 2.175 dB down from that of the initial array. This is indicative of a 36.12% improvement in performance for the regulation of sidelobe levels. For a direct impingement and the particular DoA of the desired and interfering signals in this case, a 0.02 increase in value of c corresponds to a drastic reduction in the first sidelobe level.

It is noticeable in Figure 12 that the null in the radiation pattern at 30° is indicative of the rejection of the interfering signal at its bearing angle. This highlights the performance of the SCC within the mathematical algorithm, as the optimised system is still able to reject interference from a particular direction while improving the estimation performance and sidelobe level regulation.

The length of the aperture differs only slightly from the previous simulation, being 0.1481 metres shorter. This implies that the length of the aperture remains a sensible size as c increases in value. It is noted however that the optimised array has shifted further away from the initial element positions along the negative half of the x-axis. A maximum displacement of 1.0822 metres from the initial position can be observed by the first element in the optimised linear array. While the length of the aperture remains fairly constant, it is evidenced that the entire aperture itself begins to shift away from the initial array towards the negative region of the x-axis.

7.1.3 Simulation 3: $c = 0.04$

As shown in Figure 13, the estimation performance for $c = 0.04$ remains largely unchanged, with the beamwidth decreasing in value by only 0.08°. It is noteworthy however that this increase in value of c by 0.02 now corresponds to a decrease in the mainlobe beamwidth, compared to its increase from Simulation 1 to Simulation 2. This may again be due to the algorithm's attempts at finding a set of positions that allow for a compromise to be made between improved estimation in the system and the reduction in sidelobe levels.

For this value of c, the first sidelobe level has decreased by 0.104 dB from Simulation 2, corresponding to an overall improvement in performance of 37.85% over the initial array configuration. It is evidenced that for a beam steering angle of 0°, increases in the value of c are associated with the reduction of the first sidelobe level. However, it is noticeable that for this increase in value of c for this simulation, there is only a very minor reduction in sidelobe level compared to that from Simulation 1 to Simulation 2.

Figure 13 shows that the interference direction is still being rejected, with its corresponding null in the radiation pattern at the azimuth angle of 30°. These results contradict our previous thoughts regarding the trade-off between sidelobe levels and interference nulling; the optimised system is still able to maintain the rejection criteria while ensuring the first sidelobe level remains below a given threshold corresponding to the value of $c = 0.04$.

From Simulation 2 to Simulation 3, the length of the aperture has again remained approximately constant,

with the aperture in this simulation being 6.9 millimetres longer than the previous. It is able to observed however that the optimal array has continued to shift further towards the negative region of the x-axis, with a maximum displacement of 1.2858 metres being exhibited by the first element in the optimised array. This result indicates that increasing values of c correspond to a greater shift in the optimal array from its initial element positions.

7.1.4 Simulation 4: $c = 0.08$

The reduction in the mainlobe beamwidth from Simulation 3 to Simulation 4 is markedly higher than that from Simulation 2 to Simulation 3. With a 1.068° reduction in beamwidth from the previous simulation, the overall improvement in estimation performance from the initial array correlates to 31.66%.

With $c = 0.08$, we see that the first sidelobe level is 2.336 dB down from that of the initial array. This is only a 0.057 dB decrease from Simulation 3 and much like before, with even a two-fold increase in the value of c, the first sidelobe level experiences only a very minor reduction in magnitude.

The direction from which the interfering signal originates continues to be rejected by the optimised system, however it is noticeable that the nulling effect is not as intense in this simulation, with the trace of the radiation pattern of the optimised linear array extending to only approximately -17.5 dB, compared to the -22.5 dB in Simulations 2 and 3. This is likely due to the higher masking value of 0.08 assigned to the SCC, with the system recognising the emphasis being placed on sidelobe level reduction. As a result, the positioning of the elements is such that the first sidelobe level is further reduced while still attempting to satisfy the rejection criterion of nulling the azimuth angle at 30°.

The most profound result of this simulation is evidenced by the positioning of the elements in the optimised linear array. It can be seen in Table 7 that with $c = 0.08$, the length of the aperture remains similar to the previous simulations, being 0.9633 metres longer than the initial aperture. However, it can be seen that the optimised aperture has been shifted extremely far from its initial positions, with the first element being placed 11.3495 metres away from the origin. This extreme deviation highlights the effects the SCC has on the optimisation process for $c = 0.08$. While the aperture length remains a sensible size, the position of the elements however become impractical given the relatively large deviation from the initial element positions.

7.1.5 General Discussion for Direct Impingement

The effects of the optimisation algorithm described in (28) are able to be visualised in the figures in Section 6. It is evident that the CRB and the SCC play an important role in the configuration of the array, with their intended effects able to be observed, resulting in a successfully optimised system.

Throughout the four simulations for varying values of c, we see the noticeable improvement in the estimation performance of the optimised array over its initial configuration. This is highlighted in the narrow mainlobe beamwidth depicted by the green trace in the figures above. As such, we can conclude that the optimisation algorithm is able to confidently determine a lower bound for the estimators in the system, with the Fisher information able to provide knowledge of where to optimally place the elements when given a particular DoA of a desired signal.

The reduction of the first sidelobe level across all simulations can also be observed, however it is noticed that there are diminishing returns inherent in the system. As the value of c is increased, there was an inversely proportionate decrease in the first sidelobe level. This implies that for the few antenna elements being used in the simulation, the algorithm experienced practical difficulty in determining a more optimised position than those obtained in Simulation 2. However, this is also heavily influenced by the algorithm's needs to additionally optimise the positions so that the interference direction of 30° continues to be rejected while narrowing the beamwidth of the mainlobe.

From the simulations above, it can be concluded that in the case of the desired signal impinging directly on the array, the length of the aperture remains a sensible magnitude; on average, being 0.899 metres longer than the 2 metres of the initial aperture. However, it can be observed that the entire optimised array experiences a displacement towards the negative region of the x-axis as the value of c increases. We see that for each increment of c in the simulations, the optimised array shifts further left, until eventually experiencing a maximum displacement of 11.3495 metres. For $0 \leqslant c \leqslant 0.04$, the length of the aperture and its displacement from the origin makes it a practically feasible system. If the real-world scenario called for the development of a linear array, the optimised solution presented in these simulations would allow for it to be retrofitted as a relatively low-profile device aboard existing military structures. However, in the case where $c > 0.04$, it is impractical to position the array approximately 11 metres away from the existing structure.

7.2 Oblique impingement

7.2.1 Simulation 1: $c = 0$

In Figure 15, it is evident that the estimation performance of the optimised system has been improved over its initial counterpart. From Table 10, a 11.55% reduction in the beamwidth of the mainlobe can be calculated. It is immediately obvious that this reduction in beamwidth is not as large as observed in the case of direct impingement, signifying that steering the beam of the array has an effect on estimation performance.

Since $c = 0$, the regulation of sidelobe levels is not a constraint imposed on the optimised system in this simulation. As a result, the first sidelobe level is higher than that of the initial array. This is a stark contrast to Simulation 1 in the case of direct impingement, once again signifying the effects beam steering has on the response of the system. From Table 10, it can be calculated that the first sidelobe has increased by approximately 22.54% over the original; the magnitude of the sidelobe increasing by a considerable margin.

From Figure 15, it can be shown that the optimisation algorithm has attempted to satisfy the rejection criteria while improving estimation performance. With the interfering signal originating from a bearing of 50° in this simulation, the optimised system has only partially rejected that azimuth angle in its response; the system rejecting the azimuth angle closer to 60°. This gives evidence to the fact that the algorithm finds it difficult to determine the optimum element positions that simultaneously allow for a narrow mainlobe beamwidth and the accurate rejection of a particular DoA of interference.

Table 9 shows that the positions of the elements in the optimised linear array remain very close to their initial configuration, with the maximum displacement being 0.1826 metres, exhibited by the fifth element in the array. As such, the length of the aperture remains fairly constant in comparison to the initial configuration; only being 0.1959 metres longer. Once again, this implies that the optimised array can be achieved by only making minor adjustments to the initial configuration.

7.2.2 Simulation 2: $c = 0.02$

From Simulation 1 to Simulation 2, the estimation performance has degraded, with the beamwidth of the mainlobe being 4.64° wider than previously. It is also immediately noticeable that the beamwidth of the mainlobe of the optimised array exceeds that of the initial in this simulation. This is the first case where the estimation performance has worsened with the increase in value of c.

The improvement over the previous simulation lies in the reduction in the first sidelobe level, being 1.076 dB lower than in Simulation 1. However, it still remains higher in magnitude than the initial array, this time corresponding to a 4.67% increase. Despite the level of the first sidelobe being higher than in the initial

configuration, this simulation lends credibility to the fact that as c is increased, we are able to observe a reduction in the first sidelobe level.

In conjunction with the loss of estimation performance, we also see a failure for the system to separate the interference from the desired signal. This is shown in Figure 16, where the rejection of the azimuth angle of 50° is not able to be observed. Instead, we see the edge of the mainlobe transitioning into a sidelobe at the azimuth angle of approximately 65°. This indicates that the optimised system has found it impossible to determine a set of element positions within the specified neighbourhood that are able to effectively null the interference DoA while regulating sidelobe levels and estimation performance.

Conversely to the results obtained in previous simulations, we see a reduction in the length of the aperture of the optimised linear array. From Table 12 we see that the optimised aperture has decreased by 0.0631 metres, with a maximum displacement of 0.0732 metres away from the origin, exhibited by the third element of the array. Despite the beam being steered to 30°, we see a marked improvement in the aperture, with the algorithm minimising the inter-element placement of the optimised array.

7.2.3 Simulation 3: $c = 0.04$

Figure 17 immediately presents the improvement in estimation performance obtained with $c = 0.04$. It is evident that for this simulation, the algorithm was able to determine an optimised configuration that conformed to the desired estimation performance. From Table 14, we see that there is a reduction of 15.12% in the beamwidth of the mainlobe, a significant improvement over Simulation 2.

The improvement in the estimation performance however does not translate to an improvement in the first sidelobe level. We see in Figure 17 that the sidelobe level has now climbed 1.034 dB higher than what was achieved in Simulation 2. This corresponds to an overall increase of 21.84% in the magnitude of the sidelobe level compared to the initial array. This is indicative of the system's inability to satisfy the degree of sidelobe suppression inherent within the assigned value of c. We however note the perturbation in the response of the optimised array at the azimuth angle of approximately $-50°$, where the radiation pattern exhibits a minimum response before branching into the outer grating lobe. A response such as this additionally reflects the difficulty for the algorithm to determine an optimal solution to this particular combination of DoA of the desired and interfering signals.

As the suppression of the first sidelobe was unable to be achieved, it is observed that the optimal configuration is once again able to null the inference at the azimuth angle at approximately 50°. While this is closer to 55°, this shows the trade-off that the optimisation algorithm attempts to achieve between separating multiple incoming signals into the system and the optimisation of the array's response in the form of sidelobes.

The length of the aperture of the optimal configuration is seen to be 0.2946 metres longer than its initial array, as shown in Table 14. Using the information presented in Table 13, we see a maximum displacement of

0.2205 metres, once again exhibited by the fifth element in the optimised array.

7.2.4 Simulation 4: $c = 0.08$

In comparison to the previous simulation, we see a drastic reduction in the estimation performance of the optimised array, shown in Figure 18. Similarly to Simulation 2, the beamwidth of the mainlobe far exceeds that of the initial configuration, with the optimised array possessing a beamwidth that is 4.58° wider. The radiation pattern depicted in Figure 18 shows that for the simulated value of c, no optimal set of positions could be determined that would yield an improvement in estimation performance.

With this increase in beamwidth of the mainlobe, we see a reduction in the first sidelobe level beyond that of the initial array. This is due to the algorithm being unable to find a solution set that offers improved estimation performance for the given value of $c = 0.08$, with the optimised system placing an emphasis on sidelobe suppression.

As observed in Simulation 2, the lack of improvement in estimation results in the ability of the optimised system to satisfy the rejection criteria imposed by the SCC. In Figure 18, we observe a lack of interference nulling at the azimuth angle of 50°, with this simulation depicting an immediate transition from the mainlobe to the sidelobe at the right-most edge of the aperture.

Much like before, the inability for the system to perform any sort of interference nulling results in an array that exhibits a smaller aperture than the original configuration. As shown in Table 16, we see that the optimised array exhibits an aperture that is 0.2042 metres shorter than the initial array, with a maximum displacement of 0.1921 metres for the first element.

7.2.5 General Discussion for Oblique Impingement

In the scenario where the mainlobe is to be steered to a direction other than 0°, it can be seen that in comparison to direct impingement, the system experiences difficulty optimising for the various constraints. It is able to be observed that beam steering negatively impacts the ability for the algorithm to form a viable trade-off between the CRB and SCC. As such, the regulation of sidelobe levels is found to be a challenging constraint to optimise for; likely due to how the response grows towards the edges of the aperture.

In Simulations 2 and 4, we see that for angles of arrival of 30° and 50° for the desired signal and interference respectively, the algorithm is unable to effectively improve the estimation performance, resulting in the positions of the elements yielding a lower sidelobe response compared to Simulations 1 and 3. We are able to observe however that when the rejection criteria is able to be satisfied, there is a corresponding increase in the length of the aperture of the optimised array. Conversely, when the mainlobe connects directly to the sidelobes towards the edges of the aperture, as was the case in Simulations 2 and 4, there is a corresponding

decrease in the length of the optimal array.

Given the nature of these results, it can be seen that for higher values of c in arrays subject to oblique impingement, the solution set obtained by the optimisation algorithm described by (28) offers a lack of interference nulling. The ability to separate incoming signals becomes a strenuous task for the system, as shown in Figures 16 and 18. It was observed in the scenarios where the estimation performance was able to be improved that there was a corresponding rejection of the interference at its corresponding azimuth angle.

It is able to be concluded that the algorithm is not completely effective at optimising the estimation performance while constraining signal separability and sidelobe level regulation for the case of oblique impingement. The results obtained from these simulations indicate that the masking value assigned to the SCC must be carefully considered for a particular combination of angles of arrival for the desired signal and interference in the case of oblique impingement.

7.3 Comparison to Related Works

The objectives achieved in this thesis have been the peripheral subjects of various studies throughout the literature. Having successfully developed an optimisation algorithm that can improve the performance of a uniform linear array, we compare our solution to existing notable solutions in the literature that share the goal of optimising DoA estimation using methods similar to the ones presented in this study.

7.3.1 Adaptive Array Thinning

Aboutanios et al. used the concept of array thinning in order to enhance DoA estimation. This was done using a planar array consisting of discretely spaced antenna elements. By selectively turning on and off specific sets of elements within the planar array, the physical characteristics of the mainlobe was able to be configured. In this way, the DoA of a desired signal was able to be better approximated. The formulation of which elements to be selected was conducted via a determination of the CRB, and was extended to both isotropic and directional arrays. Aboutanios et al. went further as to attempting to have the optimisation be solved in polynomial time due its inherent complexities by presenting a Dinklebach-type algorithm in conjunction with a convex relation.

It is apparent that this method is much more robust in that it first performs a coarse estimation of the desired signal's DoA, then selectively chooses which elements to switch 'on' and 'off' in order to refine the beam pattern. This is a much more versatile solution to the problem, with their planar array able to obtain a much more precise result in comparison to our constrained linear array. Consequently, the solution provided by Aboutanios et al. is much more complex in nature to the one proposed in this study. Their solution also factors in the extra dimension of elevation which has been ignored in this study. As such, by utilising a larger

number of elements than those presented in the simulation results above, the solution proposed in this thesis does not produce as optimal results as those achieved by Aboutanios et al. in their study.

7.3.2 Array Geometry Configuration

Bae et al. employed the Gauss-Newton method to optimise the inter-element spacing of a uniform linear array so as to improve DoA estimation. It was also noted by Bae et al. that non-uniformity within the array would yield improved estimation performance. Their method of optimisation is similar to the one employed in this study, whereby an optimisation process is used to constrain the positioning of the elements within an array, then using an iterative method to solve for it. Instead of using specifically the CRB and the SCC as shown in this thesis, Bae et al. instead combine the Gauss-Newton method with the minimisation process of non-linear least squares such that the search for the optimal element positioning is iterated until a relative error in the radiation pattern is less than a predefined quantity.

It was noted by Bae et al. that their solution also faced the issue where steering the mainlobe of the array to 30° resulted in high sidelobes towards the edges of the aperture; a very similar problem exhibited by our solution. However, their solution involves the implementation of 17 elements, while the low-cost ESM system utilises only 5 in this study. In the context where a minimum number of elements is desired, the performance of the solution presented in this paper proves comparable to Bae et al. if their algorithm was to optimise for a similar number of elements.

7.4 Future Work

The following subsections detail retrospective improvements and amendments that would be made to the study if efforts were to continue. The thoughts presented in this reflection were also influenced by a comparison of our solution to the existing forms from the literature.

7.4.1 Sidelobe Level Regulation

A more refined windowing function must be developed so as to improve the regulation of sidelobe levels towards the edges of the aperture. It was noted in Section 7 that the constraint imposed by the SCC was successful in reducing the magnitude of the first sidelobe level for direct and oblique impingements. However, to further distinguish the mainlobe within the radiation pattern, the sidelobe levels towards the aperture of the array must be accounted for.

This study utilised a manual windowing function so as to have its weightings optimised by the optimisation algorithm. In future, a more optimum windowing function would be used to regulate these sidelobe levels; more importantly, the ability for the window to be adjusted for oblique impingements. In this study, the

optimised array did not perform as well for oblique impingements as direct ones due to the restructuring of the windowing coefficients. This would be a significant area of study, as with an improved windowing structure, the optimisation algorithm would be able to better form a compromise between estimation performance and sidelobe level regulation without devaluing interference rejection.

7.4.2 Reflective Interference Effects

The configuration of the array in this study is of a linear nature. If efforts were to continue into the future, other configurations would be explored, such as circular arrays and other geometric shapes that would yield superior DoA estimation performance. With these arrays being retrofitted to existing military structures, the possibility of signals being reflected from the structure is high, given the metallic nature of most of the existing architectures. This would embed additional noise into the system and introduce inefficiencies in the array; resulting in undesirable performance for DoA estimation.

To remedy this, future studies would involve utilising the FEKO simulation software developed by Altair to construct a virtual model of the linear array and to map its electromagnetic signatures. With the software's ability to simulate a variety of virtual environments, this would prove invaluable in monitoring how signals would react to a multitude of surface types, allowing for adjustments to be made in the physical design of the solution.

7.4.3 Computational Time and Larger Structures

The algorithm developed in this study is able to successfully determine the optimum set of element positions within a particular neighbourhood of its search function. While the simulations conducted in this study consisted of only 5 elements, it would prove interesting to discern the results of the optimisation process for an array consisting of a larger number of elements.

To implement this, the problem would need to be reconfigured due to computation time. The optimisation algorithm described by (22) is not well behaved; with computation time increasing disproportionately as the number of variables, in the form of Lagrange multipliers, to be solved for increases. As such, it is necessary to devise an optimisation process that implements the same constraints, however has computation times bounded by the number of variables needing to be solved for. In this way, it would be possible to simulate arrays of a larger structure; potentially consisting of more than 20 elements.

8 Conclusion

With the rapid adoption of ESM systems in military applications around the world, the environments in which these systems operate are prone to saturation by EM energy originating from active radar and electronics. As a consequence, the direction and accuracy with which the DoA of a desired signal can be estimated becomes less than optimal, with the propensity to be degraded by a source of interference. Thus, the implementation of a system that is able to more optimally discern multiple incoming signals within an EM environment is necessary so as to better determine the estimation of the direction of a signal of interest.

This study attempted to derive an optimisation process that would allow us to determine the array structure that provides the most optimal performance for a particular DoA, while ensuring a minimum rejection performance to an interfering direction. To accomplish this, we sought to achieve three key objectives: to use the CRB to develop a metric for performance estimation, to incorporate the SCC as a constraint to suppress interference effects, and to apply a maximum value to the SCC in conjunction with a manual windowing function to improve the beam pattern.

The proposed solution formulated in this study was able to achieve the simultaneous optimisation of estimation performance and signal separability. The results obtained from the simulations focused on two potential scenarios: direct impingement and oblique impingement. In each scenario, the assigned masking value to the SCC is changed to observe the response of the optimised array. In the case of direct impingement, the optimised array outperformed the initial, with the optimisation algorithm able to successfully determine an array structure providing optimal estimation performance in accordance with interference nulling. However, in the case of oblique impingement, it is able to be observed that beam steering negatively impacts the optimisation process. In this scenario, the masking value of the SCC must be chosen carefully so as to result in an optimised configuration.

Simultaneously optimising for the estimation performance and the rejection of interference sources while regulating sidelobe levels is a novel combination that has not been completely explored by past authors in the literature. It is common to see past methods optimise for singular aspects, such as performance estimation or interference rejection, however, only few have attempted to develop a solution that optimises for both. In the context of the solution proposed in this thesis, an inherent weakness lies in its ability to determine an optimised configuration when the beam has been steered. This is likely due to the windowing coefficients not being optimally restructured, influencing the performance attempting to be optimised by the algorithm. If the efforts depicted in this thesis were to continue in the future, the optimisation of the windowing function would be investigated so that a more robust mechanism of suppressing sidelobe levels can be implemented for beam steering. Future prospects will also include the investigation of potential reflective interference effects from the retrofittable architectures and an improvement in the computation time of the derived algorithm.

9 Bibliography

[1] M. I. Skolnik, "Radar handbook," 1970.

[2] T. Institute of Electrical and Electronics Engineers, "Standard Definitions of Terms for Antennas," *IEEE Std. 145-1993*, 2004.

[3] H. Unz, "Linear arrays with arbitrarily distributed elements," *IRE Transactions on Antennas and Propagation*, vol. 2, no. 8, pp. 222–223, 1960.

[4] D. King, R. Packard, and R. Thomas, "Unequally-spaced, broad-band antenna arrays," *Antennas and Propagation, IRE Transactions on*, vol. 8, no. 4, pp. 380–384, 1960.

[5] R. F. Harrington, "Sidelobe reduction by nonuniform element spacing," *Antennas and Propagation, IRE Transactions on*, vol. 9, no. 2, pp. 187–192, 1961.

[6] H. Matzner and E. Levine, "Sidelobe reduction in antenna arrays with different elements," in *27th Convention of Electrical and Electronic Engineering in Israel, Israel, IEEE2012*, 2012, pp. 1–3.

[7] K.-K. Yan and Y. Lu, "Sidelobe reduction in array-pattern synthesis using genetic algorithm," *Antennas and Propagation, IEEE Transactions on*, vol. 45, no. 7, pp. 1117–1122, 1997.

[8] M. M. Khodier and C. G. Christodoulou, "Linear array geometry synthesis with minimum sidelobe level and null control using particle swarm optimization," *Antennas and Propagation, IEEE Transactions on*, vol. 53, no. 8, pp. 2674–2679, 2005.

[9] H. Wang, D.-G. Fang, and Y. L. Chow, "Grating lobe reduction in a phased array of limited scanning," *Antennas and Propagation, IEEE Transactions on*, vol. 56, no. 6, pp. 1581–1586, 2008.

[10] R. Wu, Z. Wang, D. Lu, Q. Feng, and J. Li, "Further results on peak sidelobe control in adaptive arrays," in *Radar, 2006. CIE'06. International Conference on.* IEEE, 2006, pp. 1–6.

[11] X. Wang, E. Aboutanios, M. Trinkle, and M. G. Amin, "Reconfigurable adaptive array beamforming by antenna selection," *Signal Processing, IEEE Transactions on*, vol. 62, no. 9, pp. 2385–2396, 2014.

[12] Y.-C. Jiao, W.-Y. Wei, L.-W. Huang, and H.-S. Wu, "A new low-side-lobe pattern synthesis technique for conformal arrays," *Antennas and Propagation, IEEE Transactions on*, vol. 41, no. 6, pp. 824–831, 1993.

[13] B. Ji-Hoon, K. Kyung-Tae, and P. Cheol-Sig, "Design of steerable linear and planar array geometry with non-uniform spacing for side-lobe reduction," *IEICE transactions on communications*, vol. 88, no. 1, pp. 345–357, 2005.

[14] H. Gazzah and K. Abed-Meraim, "Optimum ambiguity-free directional and omnidirectional planar antenna arrays for doa estimation," *Signal Processing, IEEE Transactions on*, vol. 57, no. 10, pp. 3942–3953, 2009.

[15] M. Smith and T. Tan, "Sidelobe reduction using random methods for antenna arrays," *Electronics Letters*, vol. 19, pp. 931–933, 1983.

[16] Y. Guo and M. Smith, "Sidelobe reduction for phased array antennas using digital phase shifters. part 1: One bit phase weighting," *Microwaves, Optics and Antennas, IEE Proceedings H*, vol. 130, no. 5, pp. 343–351, 1983.

[17] N. H. Noordin, T. Arslan, and B. Flynn, "3-faceted array with low side lobe levels using tuneable windows," in *Antennas and Propagation (EuCAP), 2013 7th European Conference on.* IEEE, 2013, pp. 600–604.

[18] M. R. Sarker, M. M. Islam, M. T. Alam *et al.*, "Side lobe level reduction in antenna array using weighting function," in *Electrical Engineering and Information & Communication Technology (ICEEICT), 2014 International Conference on.* IEEE, 2014, pp. 1–5.

[19] A. Moffet, "Minimum-redundancy linear arrays," *IEEE Transactions on Antennas and Propagation*, vol. 16, pp. 172–175, 1968.

[20] Z. Liqiang and Q. Houde, "Study on the direction finding ambiguities performance of non-uniform linear antenna array," in *Instrumentation, Measurement, Computer, Communication and Control, 2011 First International Conference on.* IEEE, 2011, pp. 789–791.

[21] A. N. Mirkin and L. H. Sibul, "Cramér-rao bounds on angle estimation with a two-dimensional array," *IEEE Transactions on signal processing*, vol. 39, no. 2, pp. 515–517, 1991.

[22] R. O. Nielsen, "Azimuth and elevation angle estimation with a three-dimensional array," *IEEE Journal of Oceanic Engineering*, vol. 19, no. 1, pp. 84–86, 1994.

[23] A. Dogandzic and A. Nehorai, "Cramer-rao bounds for estimating range, velocity, and direction with an active array," *IEEE transactions on Signal Processing*, vol. 49, no. 6, pp. 1122–1137, 2001.

Appendices

A Trust-region Analysis

This section of the appendices depicts the 3D surface plot of the trust-region analyses performed by the optimisation algorithm. The trust-regions developed for the direct and oblique impingements are shown in the figures below.

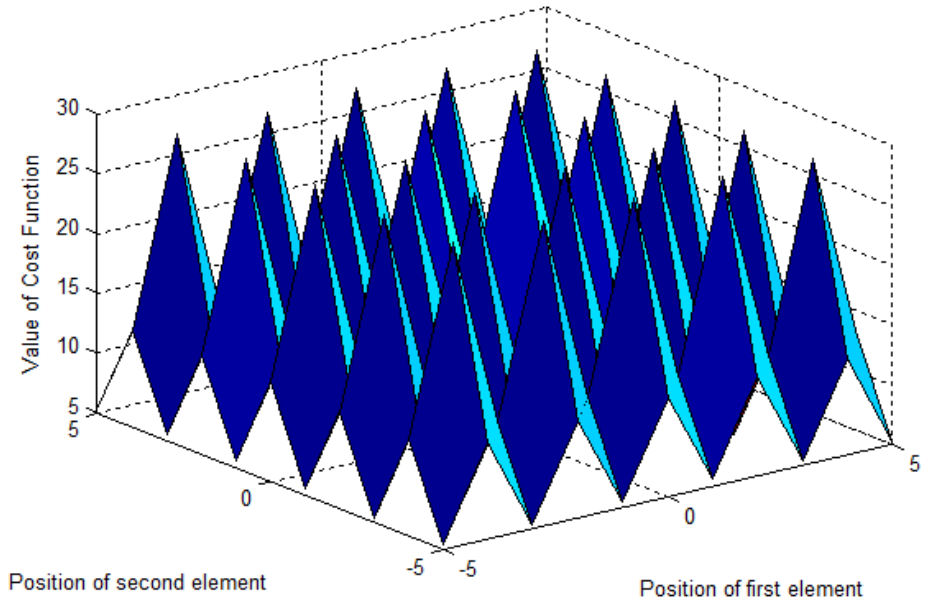

Figure A.1: Trust-region analysis in the case of direct impingement with $c = 0$.

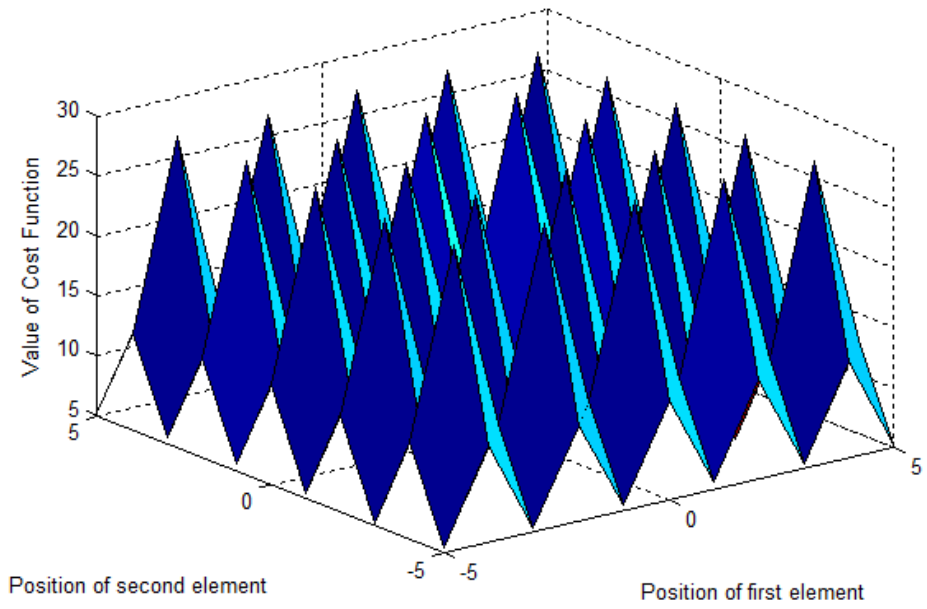

Figure A.2: Trust-region analysis in the case of direct impingement with $c = 0.02$.

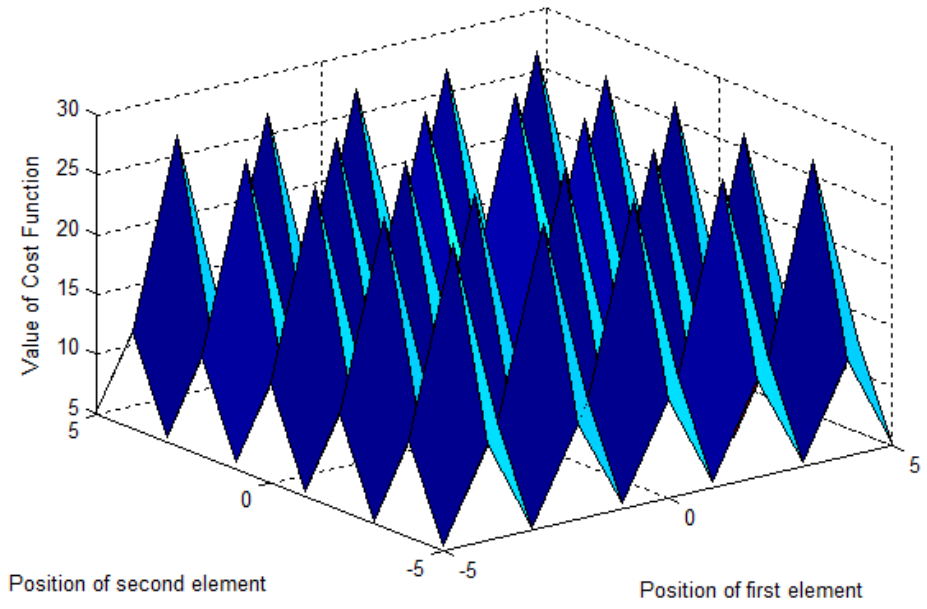

Figure A.3: Trust-region analysis in the case of direct impingement with $c = 0.04$

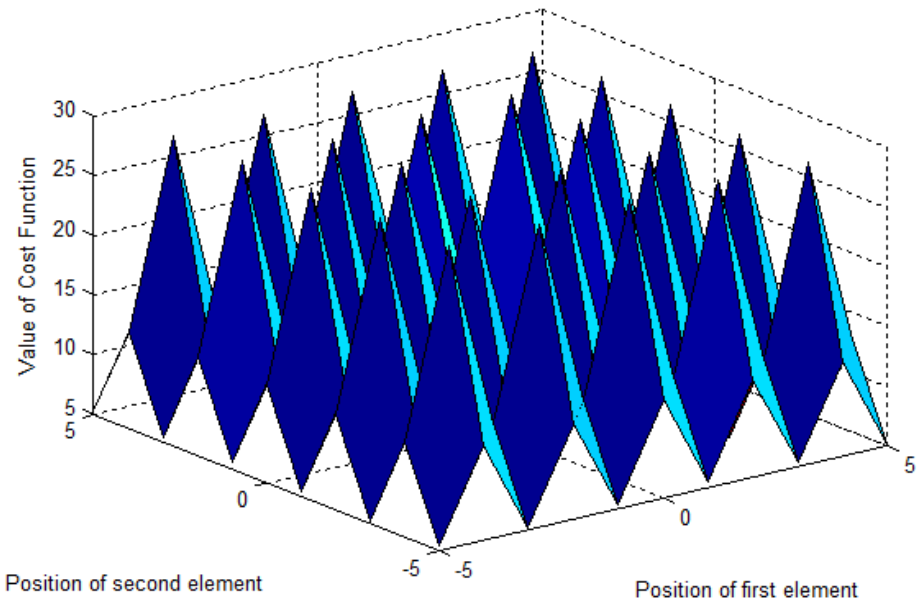

Figure A.4: Trust-region analysis in the case of direct impingement with $c = 0.08$

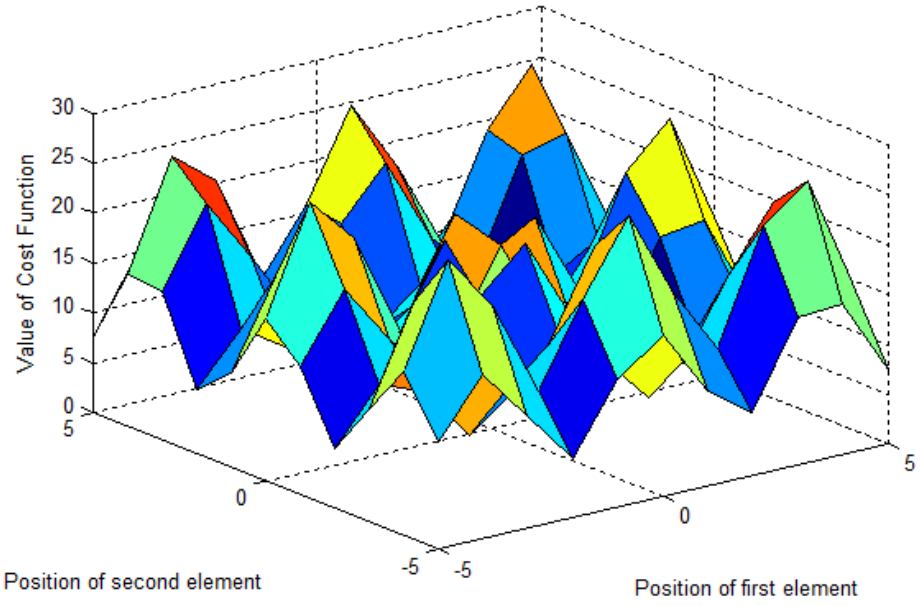

Figure A.5: Trust-region analysis in the case of oblique impingement with $c = 0$.

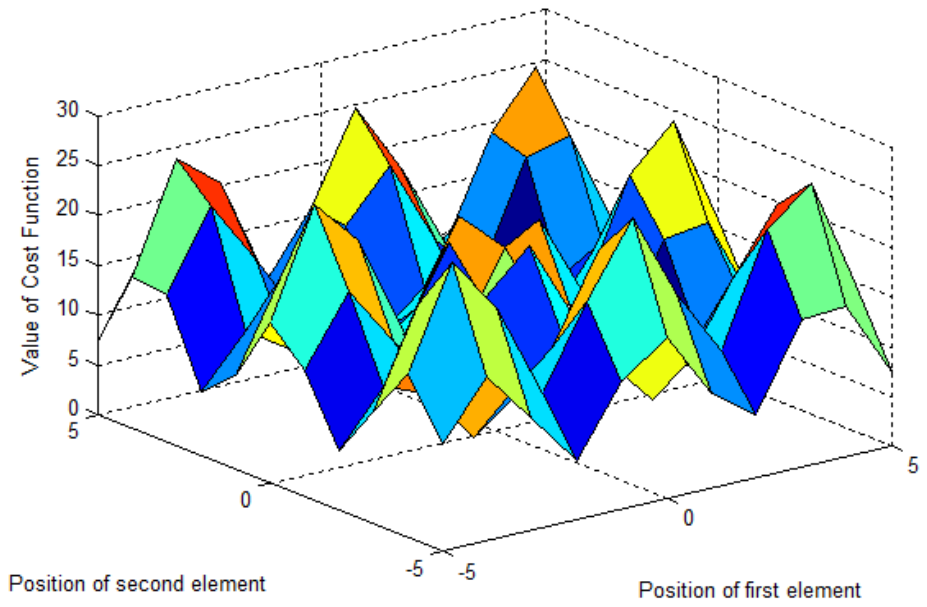

Figure A.6: Trust-region analysis in the case of oblique impingement with $c = 0.02$

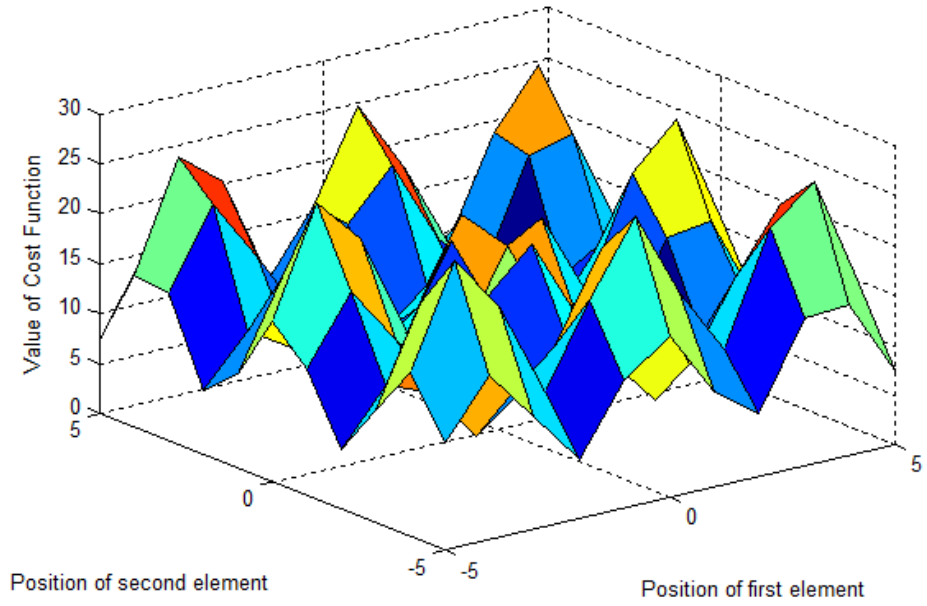

Figure A.7: Trust-region analysis in the case of oblique impingement with $c = 0.04$

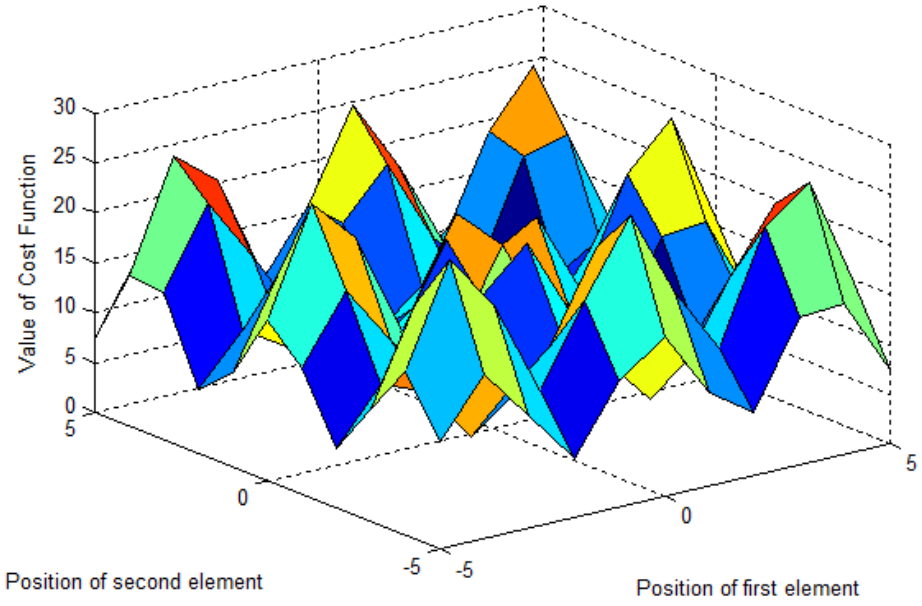

Figure A.8: Trust-region analysis in the case of oblique impingement with $c = 0.08$

B MATLAB Simulation Code

This appendix includes all of the MATLAB code that was used in the simulation of the optimisation algorithm.

```
clear all
close all
clc

fun = @root2d;
global lambda
global freq
freq = 3e8;
lambda = 3e8/freq;
d = lambda/2;

x=[-5:1:5]';

for cnt=1:length(x)
    for ccnt=1:1:length(x)
        t(cnt,ccnt)=func([x(cnt),x(ccnt),0,0,0,1,1,1,1,1,1,1,1]);
    end
end
test=t(:,:,1);
%Plot 3D surface depicting trust-region analysis
surf(x,x,test)
xlabel('Position of first element');
ylabel('Position of second element');
zlabel('Value of Cost Function');

idx=1;
for cnt=-d/2:0.01:d/2
x_stp(idx,:)=[-2*d+cnt -d+cnt 0 d-cnt 2*d-cnt zeros(1,8)];
X1(idx,:) = fsolve(@dfunc,x_stp(idx,:),optimset('display','off'))
%Checking the value of the function at this solution
fval1(idx) = func(X1(idx,:));
idx=idx+1;
end
[a b]=min(fval1)
x_f=X1(b,:)

figure,
size=length([x_stp(:,1);x_stp(:,2);x_stp(:,3)]);
sz = 100*ones(1,size);
```

```
p1=scatter([x_stp(:,1);x_stp(:,2);x_stp(:,3)],zeros(1,size),sz,'kx'),hold on
p2=scatter([-d,0,d],[0 0 0],[300 300 300],'rx'),hold on
size=length([x_f(:,1);x_f(:,2);x_f(:,3)]);
sz = 200*ones(1,size);
p3=scatter([x_f(:,1);x_f(:,2);x_f(:,3)],zeros(1,size),sz,'gx'),hold on
legend([p1 p2 p3],'Starting point','Initial placement','Solution')



function dLambda = dfunc(X)
   %Initialize the partial derivative vector so it has the same shape as the input X
   dLambda = nan(size(X));

   %The step size used in the finite difference
   h = 1e-3;
   for i=1:numel(X)
       dX=zeros(size(X));
       dX(i) = h;
       dLambda(i) = (func(X+dX)-func(X-dX))/(2*h);
   end
end



function F = func(x)

global lambda
%Arbitrary angle of desired signal
phi_s = deg2rad(0);
%Arbitrary angle of interfering signal
phi_n = deg2rad(30);

k0 = 2*pi/lambda;

%Quantisation of azimuth angle
phi_sd = -pi/2:pi/6:pi/2;
%Manual windowing function for direct impingement
delta_p = [0.001 0.01 0.1 1 0.1 0.01 0.001];
%Manual windowing function for obliique impingement at 30 degrees.
%delta_p = [0.01 0.001 0.01 0.1 1 0.1 0.01];
h=0;
for cnt=1:length(phi_sd)
  h=h+x(cnt+6)*(BeamPattern(x,phi_sd(cnt),phi_s,k0)-delta_p(cnt));
end
c=0;
F =1/(x(1)^2+x(2)^2+x(3)^2+x(4)^2+x(5)^2)+x(6)*(SCC([x(1) x(2) x(3) x(4) x(5)],phi_s,phi_n,k0)-c)+h;
```

```
function SCC_SQD=SCC(x,phi_s,phi_n,k0)
u_s = sin(phi_s);
u_j = sin(phi_n);

v_s = transpose(exp(1j*k0*x*u_s));
v_j = transpose(exp(1j*k0*x*u_j));
v_js = v_s.*v_j;

W_r=real(v_js*v_js');
SCC_SQD=ones(1,length(x))*W_r*ones(length(x),1);



clear all;
close all
clc;

% Number of antenna elements
N = 5;
% Steering direction
theta_steer = deg2rad(30);
global lambda
global freq
freq = 3e8;
lambda = 3e8/freq;
k0 = 2*pi/lambda;
% Element spacing
d = lambda/2;

%Constructing the uniform linear array
idx=1;
for n=ceil(-N/2):floor(N/2)
    x(idx) = n*d;
    idx=idx+1;
end

theta_s = -pi/2:0.01:pi/2;
x_opt = [%Insert optimised element positions here];

for cnt=1:length(theta_s)
    B(cnt)=BeamPattern(x,theta_s(cnt),theta_steer,k0);
    B_opt(cnt)=BeamPattern(x_opt,theta_s(cnt),theta_steer,k0);
end

figure;
hold on;
```

```
plot(rad2deg(theta_s),[10*log10(B)'],'r');
plot(rad2deg(theta_s),[10*log10(B_opt)'],'g');
xlabel('Azimuth angle (degrees)')
ylabel('Normalised |AF| (db)');
hold off;

axis([-90, 90, -25, 0]);
legend('Initial ULA','Optimised LA')



function B=BeamPattern(x,phi_s,phi_t,k0)
u_s = sin(phi_s);
u_t = sin(phi_t);
v_s = transpose(exp(1j*k0*x*(u_s-u_t)));

B=1/length(x)*abs(sum(sum(v_s)));
```